DESIGN AND CONSTRUCTION

OF A

MAGNETIC FORCE MICROSCOPE

A Thesis

by

SAMEER S. KHANDEKAR

Submitted to the Office of Graduate Studies of
Texas A&M University
in partial fulfillment of the requirements for the degree of

MASTER OF SCIENCE

May 2004

Major Subject: Mechanical Engineering

DESIGN AND CONSTRUCTION

OF A

MAGNETIC FORCE MICROSCOPE

A Thesis

by

SAMEER S. KHANDEKAR

Submitted to Texas A&M University
in partial fulfillment of the requirements
for the degree of

MASTER OF SCIENCE

Approved as to style and content by:

_____   _____
Joseph H. Ross, Jr.   K. Ted Hartwig, Jr.
(Co-Chair of Committee)   (Co-Chair of Committee)

_____   _____
Dimitris Lagoudas   Dennis O'Neal
(Member)   (Head of Department)

May 2004

Major Subject: Mechanical Engineering

ABSTRACT

Design and Construction

of a

Magnetic Force Microscope. (May 2004)

Sameer S. Khandekar, B.E., Walchand College of Engineering (India)

Co-Chairs of Advisory Committee: Dr. Joseph H. Ross, Jr.
Dr. K. Ted Hartwig, Jr.

A magnetic force microscope (MFM) is a special type of scanning force microscope which measures the stray field above a ferromagnetic sample with the help of a ferromagnetic cantilever. The aim of this project was to design and build a MFM head and interface it with a commercial scanning probe electronics controller with the help of an appropriate force sensor. The MFM head and the force sensor were to be designed to work at low temperatures (down to 4 K) and in high vacuum.

During this work, a magnetic force microscope (MFM) head was designed. Its design is symmetrical and modular. Two dimensional views were prepared to ensure proper geometry and alignment for the various modules. Based on these views, individual parts in the various modules were manufactured and combined for the final assembly of the head. This MFM head has many essential and advanced features which were incorporated during the design process.

Our MFM head has an outside diameter of 5 cm and thus has a low thermal mass. The head operates inside a 100 cm long vacuum can which is kept in a cold bath inside a superinsulated dewar. Other features of this MFM head include thermal compensation of the important parts, flexibility to use commercial MFM cantilevers and a large scan range compared to the previous designs. Some of the anticipated system specifications are: 1) room temperature scanning range of 175×175 μm, 2) low temperature scanning range between 35-50 μm, 3) smallest detectable magnetic force in the range of one pN and 4) smallest detectable magnetic force gradient in the range of 10^{-3} to 10^{-5} N/m.

This MFM head was interfaced to a commercial scanning probe electronics apparatus by designing a fiber-optic interferometer as the sensor for the detection of the cantilever deflection. The fiber-optic sensor also has features of its own such as stability, compactness and low susceptibility to noise because of all-fiber construction.

With this MFM head, we hope to image many magnetic samples which were previously impossible to image at Texas A&M.

ACKNOWLEDGMENTS

TABLE OF CONTENTS

LIST OF FIGURES

I. INTRODUCTION

A. ATOMIC FORCE MICROSCOPY (AFM)

The invention of scanning tunneling microscope (STM) in 1982[1] opened a new field of microscopy called scanning probe microscopy (SPM). One family of microscopes which falls under this category is scanning force microscopes (SFM). Such microscopes are based on the principle of detection of forces and hence the name scanning force microscopes. The most popular offspring of the SFM technique is atomic force microscope (AFM). It was called atomic force microscope by its inventors Binnig and Rohrer[2] because it was capable of achieving atomic resolution by detecting forces between atoms. However, later it was realized that this type of microscope can be used to analyze not only atomic forces but also various short-range and long-range interactions. The various types of forces which can be analyzed include electric and magnetic forces as well. The microscope based on the principle of detection of magnetic forces is called magnetic force microscope (MFM). It is another popular, useful and important type of scanning force microscope.

The first part (A) of this section is a discussion on AFM. The main topics discussed are force interactions between the tip and the sample and the various modes or methods of doing AFM.

The second part (B) of this section is a similar discussion on MFM.

1. Force interactions in AFM

In AFM a sharp probe i.e. a tip attached to the end of a micro-cantilever is scanned in close proximity to the sample or vice versa. In this case the interactions taking place between the end atoms of the tip and surface atoms of the sample are mainly because of van der Waals forces. These can be short-range or long-range depending on the distance between the tip and the sample. AFM is sensitive enough to detect surface forces at a nanometer scale.

This thesis follows the style and format of Review of Scientific Instruments

At a relatively large separation, long-range van der Waals interactions are evident. These lead to negative interaction potential or attractive forces. The three major factors on which these interactions depend include tip-sample material, tip-sample geometry and medium between tip and sample. The forces arising out of these interactions can be characterized by a reciprocal power law,[3] usually of order greater than 3.

If the distance between the tip and the sample is reduced further there is a possibility of overlap of electronic wave functions of the atoms of the tip and the uppermost atoms on the surface of the sample. The tip is then said to be contacting the sample and gives rise to short-range repulsive forces. If the tip to sample distance is decreased further it leads to continuously increasing repulsive forces. These forces are very short range as they occur only when the distance between the tip and the sample is of the magnitude of the radii of atoms.

The net interaction potential is the sum of the long-range and short-range potentials. The three main regions which can be identified are a. only long range attractive interactions are dominant b. short range interactions balancing the long range ones giving rise to minima c. short range repulsive forces dominate. Typically it looks as shown in Fig. 1. The extent of contact regime is typically less than 1 nm from the surface while non-contact regime can extend up to 10 nm.

AFM microscope works in three modes 1) contact (or DC mode) 2) intermittent contact (or tapping mode) 3) non-contact (or AC mode). When the working mode is the contact mode, the cantilever is in the region 'c' where repulsive forces dominate. When AC mode is used the cantilever is in the region 'a' where long range attractive forces dominate. In tapping mode the cantilever is in region 'b'.
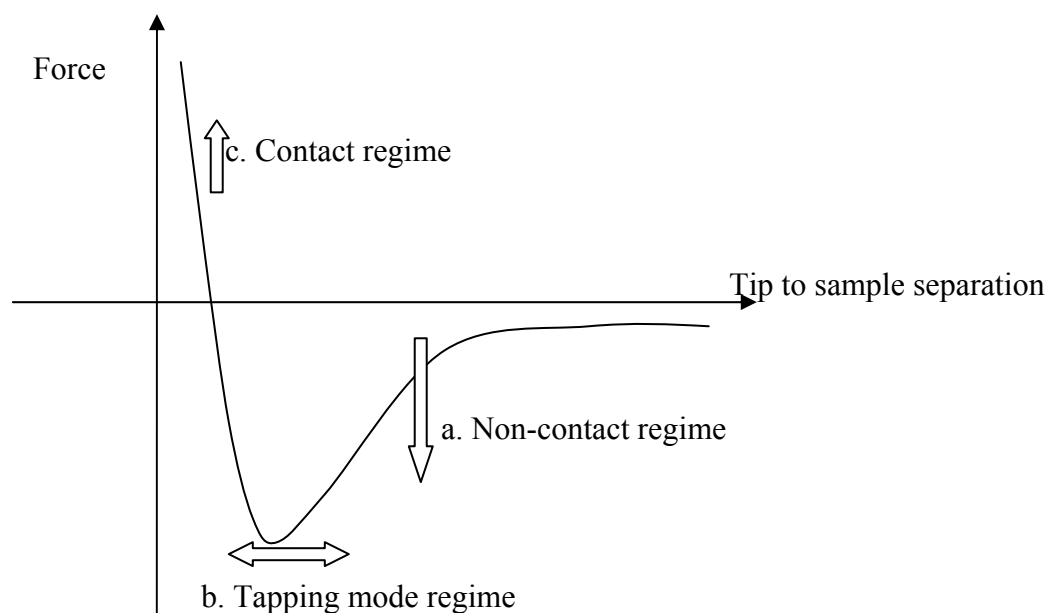
FIG. 1. Schematic representation of different regimes in AFM (not to scale, contact regime extends less than 1 nm from the surface while non-contact regime can extend up to 10 nm)

If there are other long range interactions such as electrostatic or magnetostatic interactions, they can be described by linearly superimposing them on the van der Waals potential. If there is a thin liquid layer (e.g. a water layer), other forces such as capillary, solvation and double-layer forces manifest themselves. The presence of a liquid layer can change the electrostatic interactions altogether. The total interaction in this case can not be described by linear superposition.[4]

2. Contact mode

In contact mode AFM the cantilever experiences a repulsive force. It bends like a spring. Its behavior can be described by Hooke's law which is the governing equation for contact-mode operation:

$$\Delta z = \frac{F}{K} ,$$ (1)

where Δz is the deflection of the cantilever with the spring constant K when the force acting on it is F. The principle of DC or contact mode is explained in Fig. 2.

DC bending of the cantilever
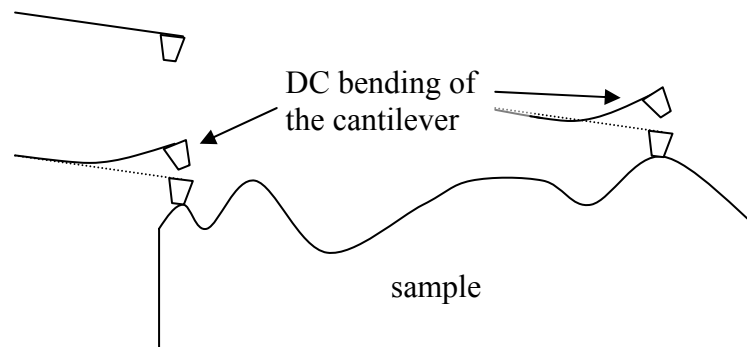
sample

FIG. 2. Operating principle of DC mode. The tip is made to follow surface topography while maintaining a constant deflection via feedback

As the cantilever is scanned across the sample it experiences a different force at each point in the scan due to the varying topography, so by monitoring the deflection of the cantilever the topography of the sample can be imaged. This is called the constant-height method because the cantilever is scanned at a constant absolute height. The other method which can be used is called the constant-force method. In constant force method, the cantilever is scanned across the sample keeping its deflection (and so the force) constant. This is achieved by means of a feedback loop. The feedback signal lowers or raises the piezo on which the cantilever sits according to the topography underneath.

Here the height by which the piezo is raised or lowered gives the topography. In the constant force method, the feedback must have sufficient time to react to the changes in the topography, so here the scanning speed is limited by feedback reaction time.

In contact mode, though the net force is repulsive, it is always the sum of the attractive force between tip and sample (electron-nucleus type interaction) and repulsive force between the end atoms of the tip and sample (electron-electron or nucleus-nucleus type interaction). The typical loading force is in the range of a few nN. The smaller the loading forces the better is the resolution. On soft samples, a large enough loading force can bring about plastic deformation (if the tip is sufficiently strong). Though undesirable while 'imaging' the sample, this feature opens up the interesting possibility of nanolithography.

3. Non-contact or AC or dynamic mode

Non-contact or AC mode works in the domain of long-range attractive forces. Here the method of detection of force is completely different than in contact-mode. This mode always works in the feedback mode. It then maps out constant force (or force derivative) surfaces. The cantilever is vibrated near or at its resonant frequency by means of a piezoelectric-bimorph or a small piezoelectric plate. When this vibrating cantilever is brought sufficiently close to the sample (in the range of aforementioned attractive forces), its resonance frequency changes. This changes the vibration amplitude of the cantilever. This operating principle is explained in Fig. 3.
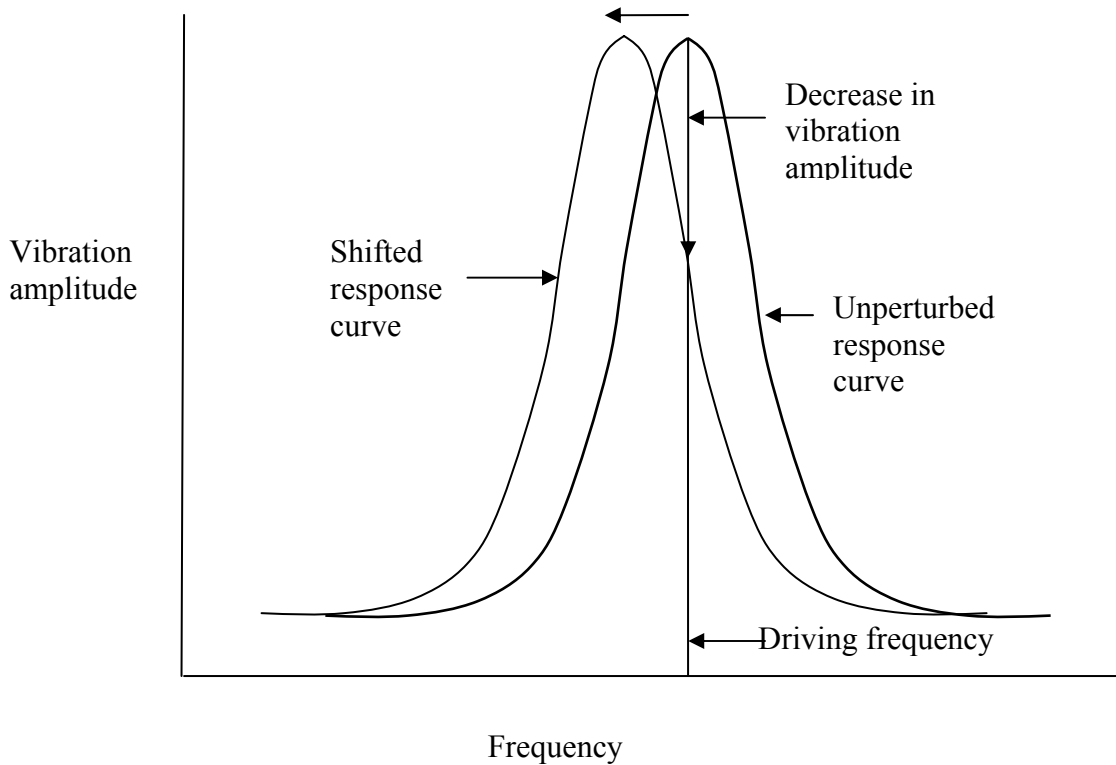
FIG. 3. Operating principle of AC mode. The interaction of tip with surface shifts the AC response curve of cantilever

As the cantilever is scanned across the sample, the feedback tries to keep the amplitude of the vibration of the cantilever constant. Similar to contact mode, this is again achieved by lowering or raising the cantilever according to the topography underneath. This height signal forms the topography image.

The governing equations for AC mode operation include the following equations (Note: These equations are nicely listed in Ref. 4) First:

$$\frac{\partial^2 d}{\partial t^2} + \frac{\omega_o}{Q}\frac{\partial d}{\partial t} + \omega_o{}^2(d - d_o) = \delta_o\omega_o\cos(\omega t), \tag{2}$$

where d is the instantaneous tip-sample distance, d_o is the tip-sample distance at zero oscillation amplitude, ω_o is the resonance frequency of the cantilever, Q is the quality

factor of the cantilever defined as $\left(\dfrac{mw_o}{2\gamma}\right)$, m is the lumped mass of the cantilever, γ is the damping factor, δ_0 is the amplitude of the forced oscillation and ω is the frequency of the forced oscillation.

Equation (2) is the equation of motion of the cantilever in the absence of interaction with the sample. However, if the distance d_o is such that the tip interacts with the sample, an additional force term has to be added to the above equation. Here,

$$F = F\left(d, \frac{\partial d}{\partial t}\right), \tag{3}$$

where d is again the instantaneous tip-sample distance and $\dfrac{\partial d}{\partial t}$ is the derivative with respect to time.

If a first order Taylor approximation is used, then the next equation tells us that the spring constant of the cantilever is modified according to the force gradient in the vertical direction

$$K_{eff} = K - \frac{\partial F}{\partial z}. \tag{4}$$

If the force gradient i.e. $\dfrac{\partial F}{\partial z}$ is positive, the effective spring constant is reduced and this softens the cantilever. If the force gradient is repulsive, the cantilever stiffens in a similar way. This changes the resonance frequency of the cantilever in the following way

$$\omega = \omega_o \sqrt{1 - \frac{1}{K}\frac{\partial F}{\partial z}}. \tag{5}$$

This equation can be approximated to give the change in the resonant frequency of the cantilever when $\dfrac{\partial F}{\partial z} << K$ as follows,

$$\Delta\omega \approx -\frac{1}{2K}\frac{\partial F}{\partial z}. \tag{6}$$

It should be noted that the force gradient which brings about the change in the resonance frequency of the cantilever does not necessarily have to be atomic. Other types of long-range forces such as electrostatic or magnetic (or more appropriately their derivatives) affect the resonance frequency the same way as described above. Thus this effect is used not only to detect atomic forces (topography) but other forces as well.

The change in the resonance frequency of the cantilever changes its amplitude of vibration according to the following equation,

$$\delta = \frac{\delta_0 \omega_o{}^2}{\sqrt{\left(\omega^2 - \omega_o{}^2\right)^2 + 4\gamma^2 \omega^2}} \quad , \tag{7}$$

where δ is the instantaneous amplitude of oscillation of the cantilever, δ_0 is the amplitude of the forced oscillation, ω_o is the resonance frequency of the cantilever and γ is the damping factor.

The change in the resonance frequency not only changes the amplitude but also the phase of the instantaneous oscillation. This can be described by the following equation,

$$\alpha = \arctan\left(\frac{2\gamma\omega}{\omega^2 - \omega_0{}^2}\right) . \tag{8}$$

The above described quantities viz. $\Delta\omega$, δ and α can be monitored to plot the lateral variation of $\frac{\partial F}{\partial z}$. The change in amplitude is usually used to detect the change in resonance frequency and is used as a feedback variable. At the same time, a map of 'phase signal' also gives important information not included in the topography signal. In most cases, it produces nice contrast at the 'edge' of features. It also gives a map of the MFM signal in both 'retrace' and 'plane scan' methods, to be discussed later.

There are two methods by which the local variation of slope can be detected. One is called 'Amplitude Modulation' or AM detection. The other method is 'Frequency Modulation' or FM detection.

In the AM detection technique, the cantilever is vibrated at or near its resonant frequency. The gradient of the force from the sample changes the spring constant of the

cantilever giving rise to change in resonant frequency and amplitude as described earlier. The changing amplitude of the cantilever as it is scanned along the sample is used as the feedback signal. This signal holds the tip-sample distance constant. This way we can measure constant force derivative profiles along the sample.

The minimum force gradient which can be measured in this case is given by,[5]

$$\left(\frac{\partial F}{\partial z}\right)_{min} = \sqrt{\frac{2KK_BT\beta}{\omega_o Q\delta_{rms}^{2}}} \,, \tag{9}$$

where K is the spring constant of the cantilever, K_B is the Boltzmann constant, T is the temperature, β is the bandwidth of measurement, ω_o is the resonant frequency of the cantilever, Q is the quality factor of the cantilever and δ_{rms} is the rms amplitude of vibration.

It can be easily seen that one of the ways of increasing the sensitivity would be to increase the Q of the cantilever. This limits the bandwidth of the measurement as the bandwidth and Q are related by the following equation,

$$\beta = \frac{1}{\tau} = \frac{\omega_o}{2Q} \,, \tag{10}$$

where τ is the approximate length of time required to settle to a new steady state oscillation value.

In the FM detection,[6] a self oscillating cantilever acts as the frequency-determining component of an oscillator (for e.g. the bimorph which vibrates the cantilever in AC mode). The cantilever is kept vibrating at its resonant frequency by what is called an oscillator control amplifier. This ensures a positive feedback to the cantilever. It also has a facility to control the amplitude of vibration at a constant level. A FM demodulator detects the changes in the oscillator frequency brought about by the change in the force gradient $\dfrac{\partial F}{\partial z}$. This signal is fed back to the piezo which controls the distance between the sample and the tip. The suggested methods for measuring the oscillator frequency are a digital frequency counter, gated timer or phase-locked loop (PLL).

The minimum detectable force gradient in this case is[6]

$$\left(\frac{\partial F}{\partial z}\right)_{min} = \sqrt{\frac{4KK_B T\beta}{\omega_o Q\delta_{rms}^{\ 2}}} \ . \tag{11}$$

This is $\sqrt{2}$ times smaller than for AM detection. It can be compensated by using a cantilever with high Q. Higher values of Q are possible in this case because the bandwidth is not limited by Q as is the case with AM detection.

4. Tapping mode

The operating range of the tapping mode varies between that of contact and AC mode. The contact mode does have potential to achieve atomic resolution. However, it exerts a relatively large force on the sample, so it can potentially destroy soft samples. AC mode applies minimum force on the sample while imaging. However,, its lateral resolution is limited by the tip-sample spacing.

The tapping mode combines the features of both modes of microcopies. Here the tip is vibrated such that it intermittently contacts or taps the surface. For most part of its oscillation the tip is off the surface. Only at the end of its motion it comes in contact with the surface and still the tip experiences the full range of interaction potential described previously. The topographic signal is still given by the amplitude signal. Here the slope changes sign as the tip enters from the attractive force region into the repulsive force region and vice versa. Thus the interaction in tapping mode is much more complicated than in above two modes.

The main advantage of the tapping mode is that the energy dissipation in this case is much lower than in contact mode. The tapping mode prevents the destruction of the sample by minimizing the shear force, as the tip is pulled sideways when it is not in contact unlike in the contact mode. Another advantage of this mode is its large, linear operating range which makes the feedback system highly stable.[7]

The resolution for the tapping mode is usually comparable or better than the non-contact mode. The choice between tapping mode and AC mode is sometimes difficult. There are no definite rules about the specific usage of any mode. As is evident in most

cases it depends on the kind of tip and sample, the medium between them and the kind of information expected from the image.

B. MAGNETIC FORCE MICROSCOPY (MFM)

Magnetic force microscopy (MFM) detects the magnetic force between a tip and a sample. This is done by using a magnetic tip which scanned across a magnetic sample (usually ferromagnetic). The adaptation of AFM as MFM was done in 1987.[8] The tip can either be made from magnetic material or a small magnetic particle could be attached to a non-magnetic tip. The most common way is to coat the tip with appropriate magnetic material. Most of the commercially available magnetic cantilevers use this method of preparation. The magnetic material could be hard such as Co or soft such as FeCoNi alloy. The selection of the magnetic material used for coating depends on its intended use. A magnetically hard coating can influence the sample magnetization but at the same time gives a strong signal; a soft coating is used to make sure that the sample magnetization is not influenced while imaging.

MFM can be carried out in two ways viz. DC mode or AC mode. The most common method is to use AC mode. When in AC mode, MFM measures the gradient of the magnetic force. In DC mode it measures the normal component of the magnetic force between the tip and the sample. In both the modes the cantilever is vibrated at or near its resonance frequency. It is the method of detection of magnetic component which separates them as DC or AC. The working of both modes can be better explained with the help of Fig. 4 which shows a magnetic force (F_m) superimposed on the van der Waals force (F_v).
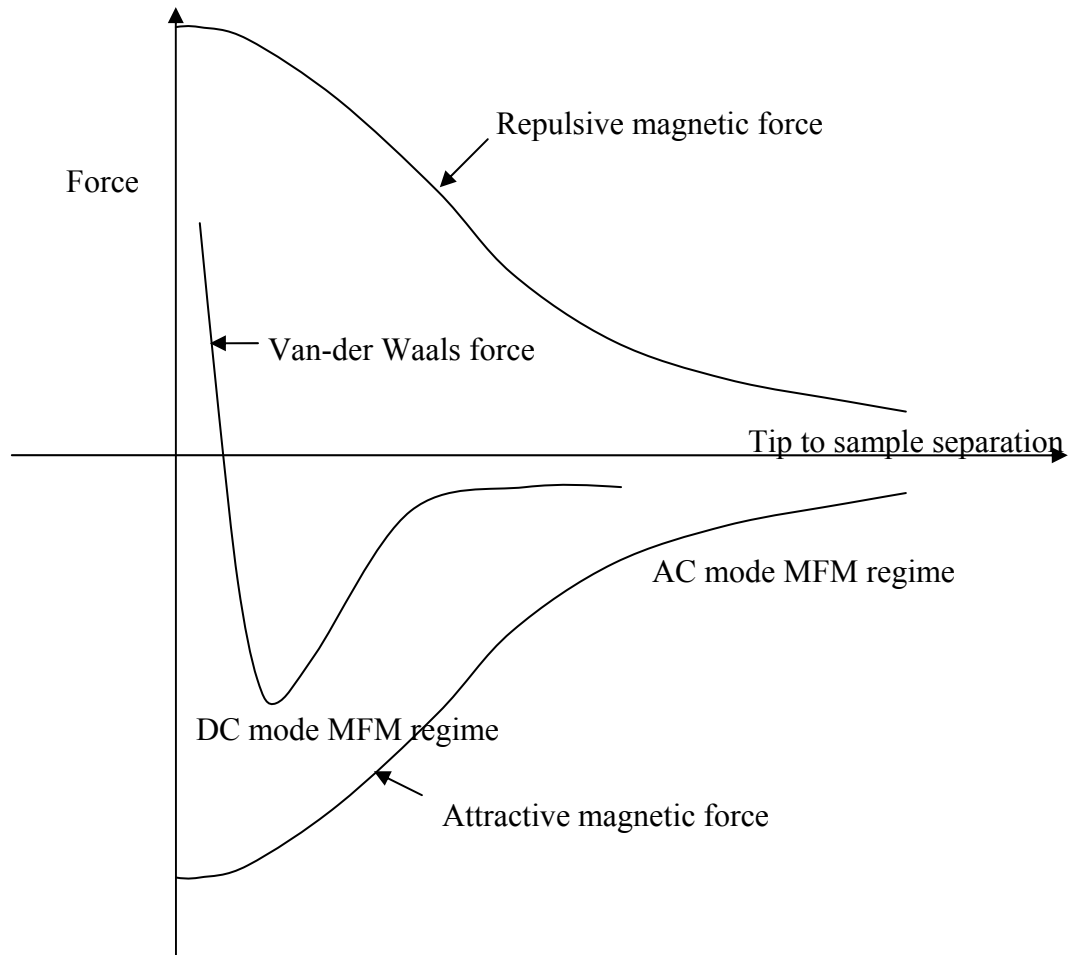
FIG. 4. Schematic view of the typical forces acting on a cantilever in MFM. Typical ranges for Van-der Waals force and magnetic forces are 10 nm and up to 100 nm respectively

1. DC mode MFM

DC mode MFM is also called near-field MFM. This works in the region where the absolute value of the magnetic force is greater than the absolute value of the van der Waals force, but the gradient of the van der Waals force is greater than the gradient of the magnetic force.[9] When the tip is scanned across a magnetic sample, it follows the variation of the normal component of magnetic force and bends accordingly. The detection of DC bending of the cantilever gives the MFM signal. Simultaneously, AC detection, i.e. the detection of changes in amplitude of oscillation of the cantilever similar to NC AFM, gives the topography signal.

Since near-field MFM involves operating with the tip close to the sample, the risk of snap-ins is much greater. One way to avoid this is to use stiff cantilevers. However, that also means reducing the intensity of MFM signal. The better way is to apply a voltage bias between the tip and the sample.[9] The absolute value of this force is much greater than van der Waals force which becomes negligible. The value of the bias is adjusted such that the overall interaction is always repulsive. In this case the magnetic signal is superimposed on the top of constant coulombic force. For near field MFM separating topographic and magnetic features can be a challenge. Applying bias helps in this regard too.

To calculate the magnetic force, the tip can be considered as a single domain with a permanent magnetic moment. With this approximation, a direct interaction between the tip and the sample magnetization ($\vec{m_1}$ and $\vec{m_2}$ respectively) can be considered. Then the normal force acting on the tip will be given by[10]

$$F(z) = \int_{tip} d^3\vec{r_1} \int_{sample} d^3\vec{r_2} \ \left(\frac{\mu_o}{4\pi}\right)\frac{\partial}{\partial z}\left(\frac{3(\vec{r}\cdot\vec{m_1})(\vec{r}\cdot\vec{m_2})}{r^5} - \frac{(\vec{m_1}\cdot\vec{m_2})}{r^3}\right) ,$$

(12)

where μ_o is the vacuum permeability and $\vec{r} = \vec{r_1} - \vec{r_2}$ inside the integral.

From the above equation it can be easily deduced that there is no normal force acting on the tip if it is scanned over a region of uniform magnetization (constant magnetic field). The forces manifest themselves when the tip approaches a domain wall separating two regions of different magnetizations. Ideally MFM would not be sensitive to the surface roughness as long as the surface roughness is small compared to length of magnetic domain of the tip (which is supposed to be equivalent to the physical length of the tip in most cases).

2. AC mode MFM

This is also called as far-field MFM. Here the vibrating cantilever is held on the order of hundreds of angstroms from the sample surface. In this region, both the absolute value and the gradient of the magnetic force dominate van der Waals force and its gradient. Thus when AC signal is read in this case it should represent the magnetic

signal and not the topography signal. Here also the application of bias between the sample and the tip is useful to ensure the dominance of magnetic force term. The other popular method to ensure that this is the case is called 'Plane Scan'. One of the first uses of this technique was to image vortices in YBCO superconductors.[11] In this method, a topographic image of the sample area is taken. Based on this image an appropriate average height is decided to raise the cantilever for the next pass. Then the cantilever is scanned over a raised plane on the sample to acquire MFM image. While doing the plane scan, the feedback is usually turned off.

AC mode detection of MFM can also be done in near-field region. This is possible because of the Retrace or Lift method. Here also two passes are made over a single line of the sample. During the first pass the topography of the sample is acquired. During the second pass, the cantilever follows the stored topography but at a greater height, so during this pass the topographic signal is eliminated. Hence it is possible to get MFM signal more easily. The Retrace or Lift method can be understood by the following simple diagram.
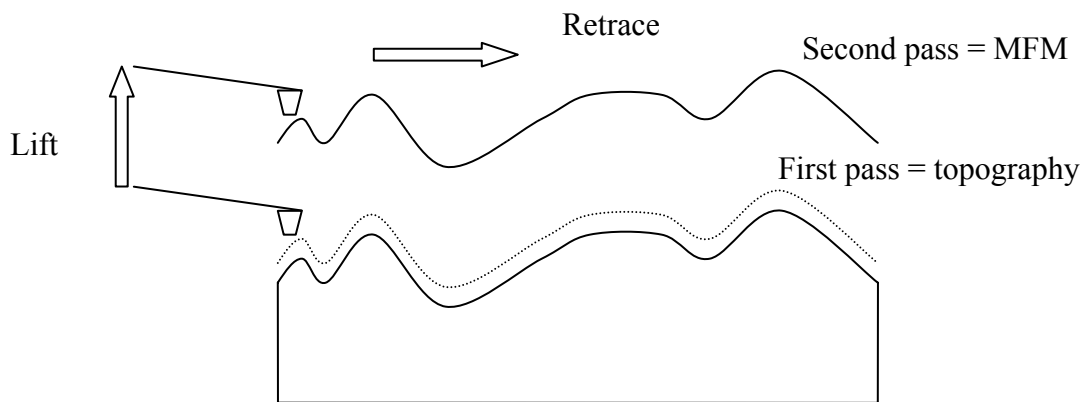
FIG. 5. Principle of Retrace or Lift mode MFM. The computer generates a second trace with the cantilever lifted to a specific height above the surface, and records the cantilever response

This is the most preferred method because it always ensures clear distinction between topographic and magnetic signals with a good resolution. It can easily image non-conducting or patterned samples. It can image soft as well as hard samples without any perturbation by choosing appropriate lift height.[11] One of its biggest operational advantages is that it is less prone to snap-ins, so this has evolved into the most preferred method of doing MFM.

To calculate the magnetic signal quantitatively, again it is useful to assume that the tip is a dipole with magnetic moment $\vec{m}$. If the magnetic field of the sample is $\vec{B}$ then the force on the tip is given by the gradient of energy which is

$$\vec{F}_m = \vec{\nabla}\left(\vec{m} \cdot \vec{B}\right) \tag{13}$$

$$= \begin{array}{l} \vec{i}\dfrac{\partial(m_x B_x + m_y B_y + m_z B_z)}{\partial x} + \vec{j}\dfrac{\partial(m_x B_x + m_y B_y + m_z B_z)}{\partial y} \\[2mm] + \vec{k}\dfrac{\partial(m_x B_x + m_y B_y + m_z B_z)}{\partial z} \end{array} .$$

If the motion of the tip is assumed to be only along the Z direction then the first two components in equation (13) become irrelevant and this expression reduces to

$$\vec{F}_m = \vec{k}\dfrac{\partial(m_x B_x + m_y B_y + m_z B_z)}{\partial z} . \tag{14}$$

If the components m_x and m_y are assumed to be zero (i.e. if the tip dipole is assumed to be along the Z direction) then the magnetic force acting on the tip can be given by the simplified expression[12]

$$\vec{F_m} = (m_z \dfrac{\partial B_z}{\partial z})\vec{k} . \tag{15}$$

The AC detection is sensitive to the Z derivative of the total force which can be written as[13]

$$\dfrac{\partial F_m}{\partial z} = m_z \dfrac{\partial^2 B_z}{\partial z^2} . \tag{16}$$

II. USES OF MFM

A. OVERVIEW

MFM when introduced as a new method of magnetic imaging was used for imaging a thin film recording head.[8] From that time, the most popular application of MFM has been the study of magnetic recording media. The higher density of data storage demands high resolution. The high resolution of MFM (20-50 nm) compared to other magnetic imaging methods is thus helpful. The fact that this method routinely gives good results under ambient conditions for bulk samples also proved to be important. There is a great deal of effort going on to develop new materials for magnetic data storage not only with high density but with controlled grain and domain structure also. MFM is used primarily to detect stray fields above such samples. There are three fundamental limitations of MFM which one has to deal with. First, the exact state of tip magnetization is unknown. Second, its fringing fields can perturb the sample. Finally, the process of obtaining sample magnetization from the mapped stray field above the sample is non-trivial. Even if the field is mapped accurately over sufficient area, the magnetization obtained from it may not be unique.[14] On the other hand; there are certain distinct advantages as well. The topographic and magnetic information can be imaged simultaneously. It is possible to understand domain structures from MFM images. The relationship of domains to grain structure can also be studied. Because of the availability of the topographic information, the influence of surface defects and morphology on magnetic information can be studied. The mapping of stray fields alone is also important in many cases.[15]

There are various possibilities when doing MFM imaging. Initially researchers used various home grown films to test the capabilities of MFM. These included CoPt tracks defined on Si by e-beam lithography,[9] TbFe and TbFeCo magneto-optic media.[16] The thin film Permalloy which is an important soft magnetic material was imaged to see closure domains and Bloch lines.[17] The domain walls in various materials like NdFeB and CoCr[18] were studied. D. Rugar et al.[19] tried to study the 'erase band' associated with overwrite behavior. They used high density CoSm on textured Al and particulate γ-

Fe_2O_3 in polymer binder. Kuo et al.[20] also used MFM to study erasure of bit transitions in high density particulate media. They used zip disks for the same. In particular, they studied the avalanche dynamics theory that had been proposed. All these researchers helped to find techniques to overcome the problem of separation of topographic and magnetic data. Also many quantitative models were developed to explain the results.

MFM was also used to study the relation between recorded magnetic structures and the reproduced noise properties on CoCrTa media.[21] The effect of different thickness and Cr concentration on the quality of CoCrTa media was also looked at.[22] It was found that increased medium thickness broadens the transition width and increasing Cr concentration decreases the remanence. A similar study involving epitaxial Ni/Cu thin films was also done. Here Bochi et al.[23] investigated magnetic anisotropy as a function of Ni thickness and alloy composition. R. Giles et al.[24] performed MFM on a computer hard disk in liquids. The purpose was to simulate the real environment for technological and biological processes. High density recording media were studied in the presence of magnetic fields as well.[25] Various stages of bit erasure were noted for different values of applied fields. Also it was proposed that the orientation of the tip can be controlled and coercivity can be obtained in situ by measuring the hysteresis loop. Magnetization reversal mechanisms in individual barium ferrite particles were studied.[26] These measurements were used as a basis to investigate their nucleation and intrinsic switching modes.

MFM was used also for sensing dynamic effects of thin film recording heads. The stray field of such heads was mapped while passing A.C. current through them.[27] Sensing of stray fields by MFM is useful because the tip experiences the same fields as does a read head. Another use was to see the effect of localized magnetic field created by the tip on the poles of the recording head. The Bloch wall motion because of the tip magnetization was also observed. Imaging of magnetically soft thin films is useful for the characterization of magneto-resistive heads. Garnet films, a kind of soft magnetic material, are technologically important for bubble type memories. These can also be investigated by MFM. There are many other phenomena involving magnetic materials

which have been studied and are being studied by MFM. It is impossible to cover all of them.

Below are given some of the examples of the MFM imaging done at room temperature in Dr. Ross' lab. The topographic image and the MFM image are both acquired at the same time using retrace mode. The magnetic force microscope used was a commercially available MFM from Nanotec Electronica, Spain.

Fig. 6 shows the MFM images of two different hard disks. The difference in the size of the magnetic domains is evident in this case with the new hard disk having smaller domain size and the old hard disk having the larger domain size.
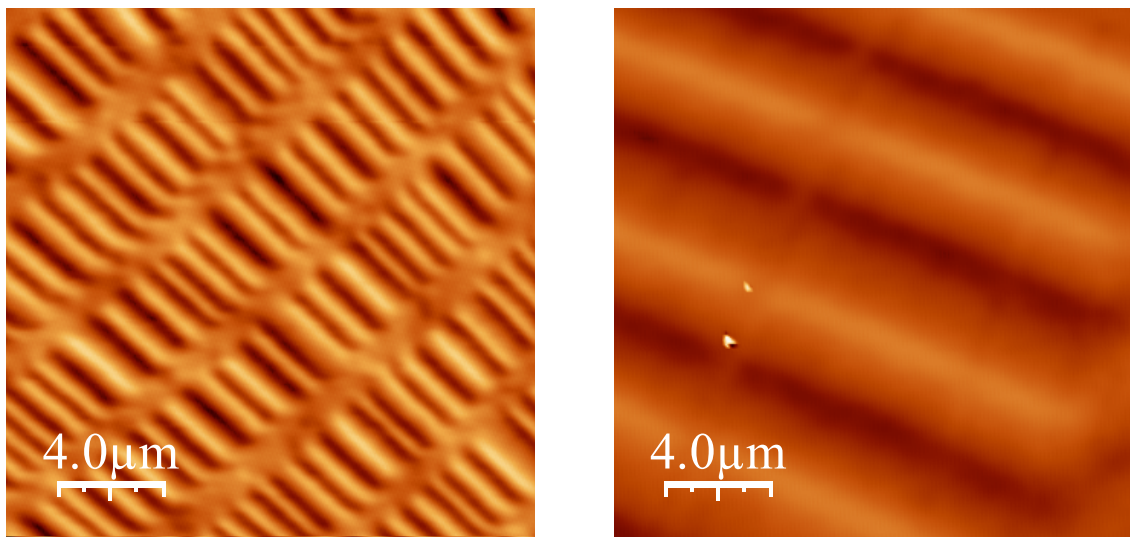
FIG. 6. MFM images showing the difference in size of the magnetic domains in two hard disk samples, new and old respectively

Figs. 7, 8 and 9 show topographic and MFM images of different regions in Co-Ni-Al smart materials (sample courtesy of Dr. Ibrahim Karaman from Mechanical Engineering Department, Texas A&M University).
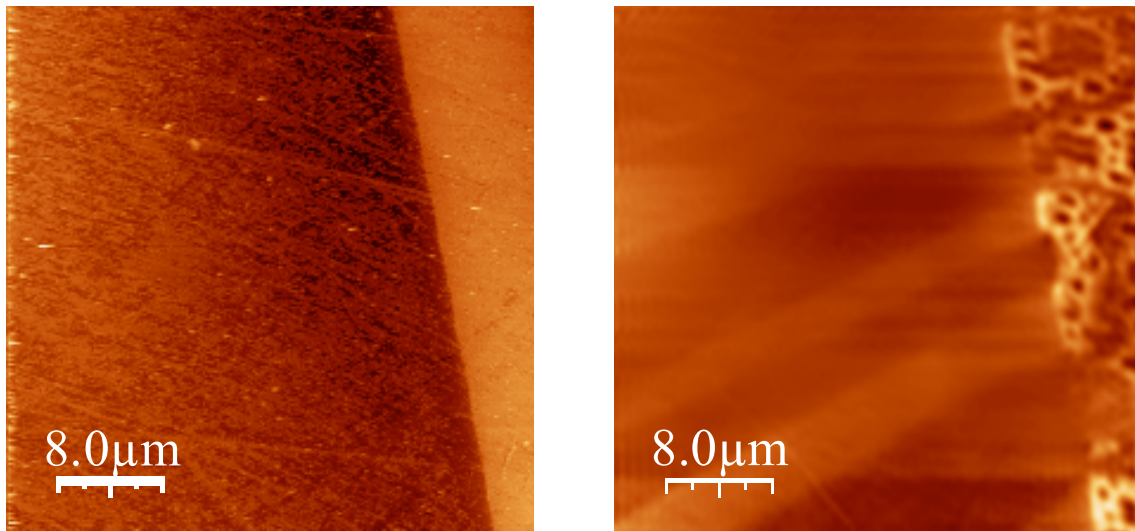
FIG. 7. Topographic (left) and MFM (right) images of a martensitic twin in Co-Ni-Al smart materials
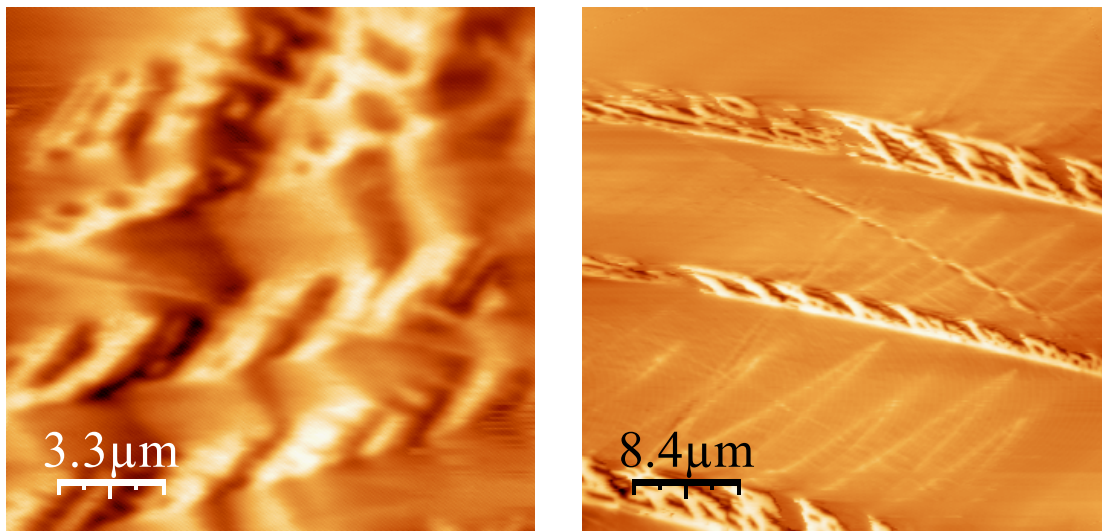
FIG. 8. MFM images of two different regions in Co-Ni-Al sample showing a series of martensitic bands
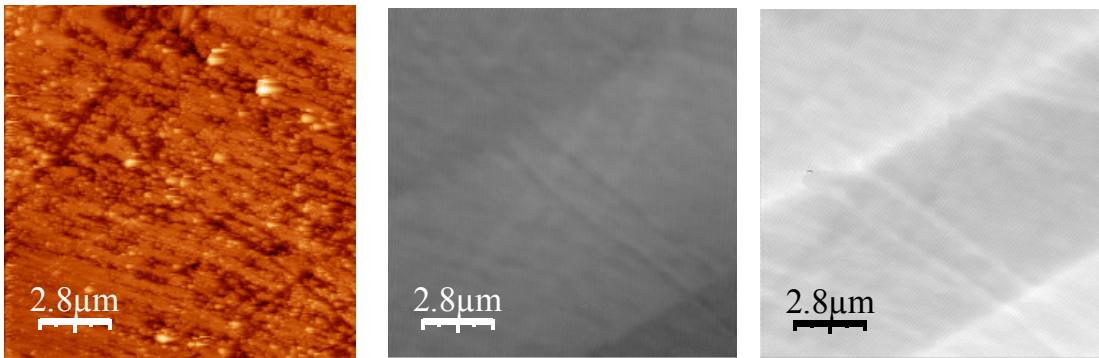
FIG. 9. Left to right: topography, MFM with no field applied, and MFM in the presence of a
magnetic field, for the same region of a Co-Ni-Al sample

Apart from these, there are certain unique MFM applications have evolved along
with the better understanding of MFM in recent years. MFM based current contrast
imaging (CCI) is a contact-less tool for observing internal circuit function and failure
analysis of integrated circuits. It is very useful for studying voltage influence of biased
interconnection lines in ICs.[28] MFM may prove useful for imaging biological samples
such as magnetotactic bacteria. Earlier studies in the fluid environment are the
foundation for these studies. A new tool developed for imaging active or live heads is
High Frequency MFM (HFMFM). It allows detecting frequencies up to 1 GHz. DI has
patented the modulation technique to separate the low and high frequency MFM
response in this case. This facilitates probing of frequency dependence of magnetic
samples with the same spatial resolution as of MFM.[29] Two other new techniques
patented by DI are Magnetic Dissipation Microscopy (MDM) and Magnetoresistance
Sensitivity Mapping (MSM). MDM probes energy losses associated with cyclic and
hysteretic perturbation of sample. With MSM, the MFM probe can be used as field
source that excites the MR sensor in a recording head. Then the symmetry and
sensitivity of GMR sensors can be investigated.

There are more recent techniques using MFM which truly use the resolution
capabilities of MFM. The magnetizations reversal of two-dimensional arrays of parallel
ferromagnetic Fe nanowires embedded in nonporous alumina templates have been

studied.[30] Isolated single molecule Mn_{12} magnets (SMM) on the surface of polymeric nanocomposite have been observed.[31] Imaging of carbon nanotubes in high performance polymer composites has also been tried. The rapid examination of the dispersion of carbon nanotubes into polymer composites is of particular interest.[32] MFM is proving to be an invaluable tool in the field of nanotechnology which makes it indispensable for nano scale magnetic work.

The low temperature use of MFM (LTMFM) can be considered as a separate field. There are numerous advantages of doing LTMFM one of which is improved SN ratio due to reduced thermal fluctuation and phonon scattering. Chung et al.[33] have used LTMFM images to show the paramagnetic to ferromagnetic phase transition in $La_{0.7}Ca_{0.3}MnO_3$ film on a $LaAlO_3$. They also examined evolution of magnetic domains and magnetic ripples near the edge of Co film on a Si substrate. H. J. Hug et al.[34] studied magneto optical disks with LTMFM. The real advantage of LTMFM is that it is able to look into superconducting phenomena which occur only at low temperature. Numerous phenomena in this field have been studied until now. It has helped greatly to improve the knowledge about superconductivity. This application of MFM has been discussed below.

B. MFM ON SUPERCONDUCTORS

The levitation of a magnet over a superconductor is a well known phenomenon. It manifests itself because of the Meissner effect. The magnetic tip also experiences a repulsive force on a superconductor. This was the principle used to investigate superconductors initially. One motivation to use MFM instead of STM was that MFM does not require a conducting surface. This factor proves significant for imaging of high-T_c superconductors. To my knowledge, the first such study was performed by A. P. Volodin et al.[35] This group did measurements on the conventional superconductor Sn and type II BSCCO. They recorded the deflection in the cantilever (due to a repulsive force) positioned relatively far away from the sample as it was cooled at the onset of superconductivity. Also the different values of repulsive force between the tip and the sample were noted as a function of tip height. This long range interaction was noted to have logarithmic distance dependence rather than the estimated reciprocal power law.

Also there were some perturbations in the measurements which were attributed either to structural defects or penetration of magnetic field of the tip into the sample. A similar study was done by H. J. Hug and A. Moser et al., [36, 37] but they used YBCO single crystal. They also showed a decreasing value of the repulsive Meissner force with increasing temperature. They also did some measurements to distinguish between the Meissner and Shubnikov phase. They were able to do so by noting the different nature of the force response from these two phases as predicted previously. It is interesting to note that levitation of a magnet over a type II superconductor between Hc_1 and Hc_2 was successfully shown as early as 1988.[38] This group also presented the theory which calculated the levitation force based on either complete flux penetration or expulsion.

The next step was to image vortices by MFM. The vortices are technologically important because motion of vortices causes dissipation. This results in lowering of the critical current, a highly undesirable effect in many applications. With vortices, STM could not give reproducible results on HTSC materials because STM is susceptible to chemically degraded surfaces. The complex structure and short coherence lengths of the superconductors and high mobility of vortices adds to the complications. The detection of a vortex via MFM was deemed feasible because a vortex has a large penetration depth and thus large magnetic diameter. The vortex bundles were imaged by using tunneling stabilized MFM.[39] The first successful attempt to image an individual vortex was in 1995 on an YBCO thin film at 77 K.[40] Not only did they observe vortices but also found that their number increases linearly with the applied magnetic field. They calculated the value of the flux carried by each vortex which was very close to one fluxon ($\phi_0 = 2 \times 10^{-7}$ Wb). They also showed that depending on the direction of the external field the interaction between the tip and a vortex could be either repulsive or attractive. By observing a stable vortex glass phase, they were able to conclude that no vortices were nucleated or dragged around by tip. This is a point of concern for MFM measurements of vortices. They also calculated the lateral force on the vortex exerted by the tip based on their earlier theoretical work.[41] In this work, they had improved upon the earlier model which assumed complete screening of flux by the superconductor. They

found that the lateral force exerted by the tip was almost two orders of magnitude less than the typical valued of the pinning force which is given by

$$F_p = j\phi_0 d \,, \tag{17}$$

where F_p is the pinning force, j is the critical current density and d is the thickness of the film. Using the London model, they also calculated the magnetic diameter of a vortex at 77 K. Yuan et al.[42] also studied YBCO and BSCCO thin films made by laser ablation and MBE respectively. They imaged vortices with radii of around 1 μm, a value greater than expected. They attributed this to the thin film factor of $2\lambda/d$ and the spreading of magnetic field above the sample. They also observed some correlation between the topographic defects and the pinning site. There were two surprising results in their study. One, instead of seeing a vortex as a circular or elliptical shape, they found some associated internal structure. This was attributed to the tip being a hard magnetic dipole with a fixed magnetic moment independent of the local field, with its axis tilted away from the surface normal. Second, they observed vortices in YBCO film at a temperature of 78 K which is very close to its T_c (81 K). This was attributed to flux trapped by some strong pinning sites. They were able to notice the movement of the vortex after a contact mode topography scan.

The observation of an Abrikosov vortex lattice was reported in 1998 in $NbSe_2$ superconductor.[43] Apart from the problem that MFM tip can drag weakly pinned vortices, the other problem to overcome was the decrease of the MFM contrast due to overlap between magnetic fields of neighboring vortices. This group used tips with a double layer coating which has been shown to improve the contrast. The flux line lattice spacing of the Abrikosov lattice they measured was very close to the theoretical value.

They also showed the change from irregular vortex lattice structure to the Abrikosov lattice structure with increasing magnetic fields. At high fields, there are more number of vortices and so their mutual interaction decides the lattice shape rather than individual pinning sites. The ability of imaging vortices at relatively weak magnetic fields was attributed to the collective pinning effect. Here all the vortices within a single domain counteract collectively the force exerted by the tip of MFM. Moser et al.[11] did

further studies on YBCO thin films. Here they imaged the single vortices and also determined their pinning centers. They found that the vortex positions were determined by pinning centers rather than by vortex-vortex interactions. The vortices were pinned at grain boundaries, as was confirmed by correlating topographic and magnetic image. They showed decreasing contrast in imaging of vortices due to increasing λ with the increasing temperature. Forced motion of vortices was achieved by using the MFM tip to apply a dragging force greater than the pinning force. Also a vortex bundle consisting of 50 vortices was nucleated by cooling the sample in the field of the tip. It was remarked that three types of control experiments 1) measurement of the dependence of number of the vortices on external field and calculation of flux associated with each vortex 2) disappearance of vortices with the temperature increasing beyond T_c and their re-nucleation 3) exhibition of attractive or repulsive interactions depending on the external field, must be done every time to ascertain that the images are indeed of vortices.

Volodin et al. further studied the evolution from a disordered towards an ordered state of vortex lattices.[44] In thin Nb films, they observed an irregular vortex arrangement with strong random pinning. However, on $NbSe_2$ they found a change from disordered to the ordered state which was attributed to collective pinning. The attempt to image growing vortex lattice grains with increasing magnetic field was not successful because of the limitation on the scan size. Also they found the vortex density slightly greater than expected value of B_{ext}/ϕ_0. It was explained with the help of the existence of an offset field because of the tip. This was confirmed by the data taken in zero field.

Recently some additional experiments have been done to study the vortex pinning. The vortex has a normal core with a size comparable to that of the coherence length. The vortex pinning is usually achieved by overlapping these with the defects in the superconductor. A spatially random distribution of defects is not so efficient to optimize the pinning. Therefore nano-engineered regular pinning arrays are better for this purpose. The long term motivation to do so is to verify how the quantum confinement of vortices results in increased critical currents and fields in the superconductors.[45] Roseman and Grutter et al.[46] investigated a superconducting Nb thin

film patterned with a square array of antidots. They observed lattice matching as a function of applied magnetic field and temperature, up to the third matching field. At the matching field, the lattice spacing becomes commensurate with that of antidots so that most of the vortices get trapped in antidots as quantized fluxons. In another study,[47] the same authors estimated the values of magnetic penetration depth of a similar sample (conventional superconductor) using constant height MFM. This was significant because uptil now only HTSC superconductors were used for this purpose. The fact that the radius of a vortex is not in general equal to the penetration depth but is instead a function of Ginzburg-Landau parameter $\kappa = \lambda / \xi$ was also taken into account. There was some discrepancy between the experimental and theoretical results. This was attributed to the fact that the observed vortex profile is a convolution between the vortex stray field and the extended tip geometry. Van Bael et al.[48, 49, 50] studied vortex pinning by ferromagnetic pinning arrays. The different possibilities of ferromagnetic structures were considered in combination with a low T_c type-II superconductor. MFM was particularly used to characterize the magnetic patterns. Other measurements such as of critical current were done by bulk methods.

Roseman et al.[51] determined the T_c of a superconducting Nb film with MFM. It is known that the resonance frequency of the cantilever changes due to the gradient of the repulsive Meissner force. In this study the sample was cooled below its T_c and the jump in the resonance frequency was recorded. This directly gave the value of T_c. Vortices were nucleated by bringing the tip close to the sample. The nucleation was evident because of the reduction in the resonance frequency of the cantilever due to attractive interaction initiated because of the nucleation of a vortex. It was remarked by the authors that the theoretical work needed to recreate the experimental data was non-trivial. They also confirmed the linear variation of the number of nucleated vortices with the applied magnetic field. Volodin et al.[52] studied vortex pinning at grain boundaries in superconducting Nb and YBCO thin films. They were able to identify the exact location of vortices within 10 nm by taking into account the asymmetry of the magnetic charge of the tip. In Nb films the preferential pinning at locations between the grains was more

pronounced for thinner films. In thicker films, on the other hand, vortex-vortex interaction seemed to dominate. They were able to see an ordered Abrikosov lattice in thicker films. It was stated that the pinning mechanisms in Nb and YBCO are different because of the difference in their coherence lengths.

In conclusion, MFM studies of vortices have opened up many interesting possibilities. In situ nucleation of vortices is interesting. The dependence of penetration depth on the temperature is an important parameter to study to test superconductivity theories. The motion of vortices and dissipation therein will also give some interesting results in the future.[53]

III. METHODS OF FORCE DETECTION AND DESIGN OF FIBER-OPTIC INTERFEROMETER

A. DIFFERENT FORCE DETECTION SYSTEMS

There are numerous techniques for detecting the deflection of the cantilever and ultimately detecting the force. These methods have evolved over a period of time. The first method used was electron tunneling.[2] Later other methods such as optical (including beam-bounce and various types of interferometric systems) and piezoresistive detection were developed. All of these techniques have merits and demerits with respect to complexity, sensitivity, low-frequency stability, types of cantilevers that can be used, compatibility with different microscope set-ups and environments and the applicability to the two modes of force microscopy. Some of the most commonly used methods are discussed below in short. The comparison with each other is presented wherever possible.

1. Tunneling detection

The working principle of tunneling detection can be explained as follows. A tunneling tip is positioned at the back of the force sensing lever. The distance between the tip and the cantilever is on the order of a few angstroms and it is controlled precisely throughout. The tunneling tip is also sometimes called auxiliary conducting tip. The application of a bias voltage between the tunneling tip and the lever produces a tunneling current through the air gap separating the two. The deflection of the cantilever varies the distance between these two, so the current variation is a measure of the lever deflection. This variation is similar to the variation of current which occurs in an STM experiment. This current is used to track and control the position of the lever (i.e. for feedback) producing an image of the force distribution across the surface of a sample.[54] A great importance is attached to this method because of its original design during the invention of first AFM. Also this was the first method to map atomically resolved insulating surfaces. This method is suitable for low temperature systems as well because it dissipates very little energy.[55] The tunneling detection can be further classified according to the geometrical arrangement of the tip and the lever. The arrangements could be

perpendicular, crossed, parallel or serial. The tunneling current density j, used for tracking and positioning the lever, can be approximated by

$$j = \frac{2\pi e^2}{h} \frac{\kappa_o}{4\pi^2 z} V \exp(-2\kappa_o z) \,^{[56]},$$

(18)

where e is the electronic charge, κ_o is the inverse decay length of the wavefunction density outside the surface, V is the bias voltage, z is the effective tunneling distance in angstroms.

The problems associated with the tunneling detection are numerous. The current between the tunneling tip and the force sensing lever depends on the presence of a medium in between them, so the presence of contamination on either of them introduces irregularities in the measurement. It is very difficult to control and position the tip accurately. The tunneling tip drifts towards the force sensing lever and eventually measures the topography of the lever, so the other methods developed use non-conducting, remote sensing and time averaging techniques to overcome these drawbacks.[54]

2. Piezo-based detection

The force detection methods based on piezo effects fall into two categories viz. piezoelectric[57] and piezoresistive methods. Out of these, piezoresistive methods are more popular. These have been used at UHV[58] and at low temperature.[59] The piezoresistive method is explained below.

2.1 Piezoresistive detection

The basic principle behind piezoresistive detection is the bulk piezoresistive effect demonstrated by silicon. Here the microscopic cantilever itself is made such that one of its layers is made of doped silicon which is a piezoresistive material. Such a cantilever can be micro fabricated. This cantilever forms one arm of the external Wheatstone's bridge.[60] The deflection of the cantilever changes the resistance of the cantilever and so the voltage across the bridge. This voltage is used to drive the feedback

and to map the images. This method is suitable for both DC and AC mode of detection. The sensitivity is also comparable to that of other methods.

The obvious advantage with this method is that it does not involve any external detection scheme. The method is very simple and reliable. One of the unique advantages it has is that it is suitable for imaging photosensitive materials, like semiconductors. The optical detection methods in this case can strongly perturb the surface properties.[61] The micro cantilevers can be batch fabricated, so it is economical to build these integrated sensors.

Due to manufacturing limitations, there is a limited range of available spring constants and resonance frequencies with these types of cantilevers. Also with these types of cantilevers there is always a concern because of relatively higher power dissipation.[43] The application of this sensor to UHV is not so straightforward if UHV preparation of the cantilevers is intended.[62] This makes piezoresistive cantilevers less attractive for cryogenic work.

3. Optical detection

The optical detection systems can be divided into beam-bounce and interferometric detection. The interferometric systems can be classified into homodyne (non-fiber, fiber coupled or all fiber) and heterodyne (non-fiber or fiber coupled) detection schemes. A short description of each method is given in this section while all-fiber type is discussed in some detail in the next section. The optical detection scheme is capable of monitoring the vibration amplitude of lever of several hundred angstroms, which is difficult to do with the tunneling technique because of the close proximity of tunneling tip to the vibrating cantilever.[63]

a. Deflection detection or beam-bounce detection

This system falls under optical detection systems. It is the most common detection system in room temperature heads. The room temperature Nanotec commercial system in Dr. Ross' lab uses beam-bounce detection and was used to acquire the images shown earlier. The working of beam-bounce detection can be explained with the help of Fig.10.
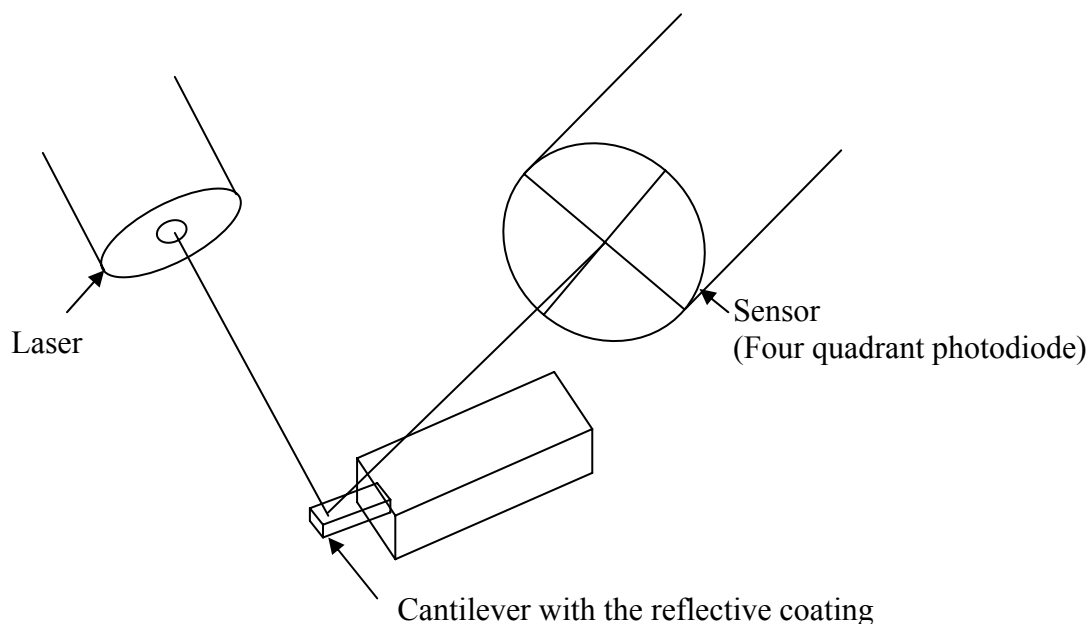
FIG. 10. Schematic of the beam-bounce detection method

A collimated laser beam is focused at the back of the force sensing lever and allowed to reflect back. The reflected beam is used to generate the photocurrent with the help of photo detectors. In the earlier versions two closely spaced diodes were used for this purpose. In the recent systems a single photodiode with 2 or 4 quadrants is used.[64, 65] The deflection of the lever as it is scanned across the sample shifts the position of the reflected laser beam across the photo diode active area. This causes change in the photocurrent proportional to the lever deflection and force. To make the back side of the cantilever more reflective, it can be coated with aluminum or gold. There are two steps necessary to make the deflection detection operational every time an experiment is done. First the laser beam has to be adjusted accurately at the back of the cantilever. Usually this is done with the help of an optical microscope. Then the photodiode position is to be adjusted to receive the maximum intensity.

One of the advantages of this system is that all the optical elements are at a large distance from the lever, so they are protected from tip crashes unlike in tunneling

detection. The other major advantage comes with the use of 4 quadrant photodiode. Here the vertical movement of the laser beam gives the value of the 'normal force' while the horizontal displacement corresponds to the 'shear force'.[66] This opens up the interesting possibility of shear force microscopy which is unique to this system. Usually normal and shear force values are measured simultaneously with different channels. The deflection detection system is stable compared with the tunneling system. The position control is much simpler. It has a large magnification because of the macroscopic optical path. It can be used for imaging in fluids.

The problems associated with this system include thermal and mechanical drifts. There is always some noise from the stray reflections of the laser beam from the sample. It can be minimized by using low coherence length laser source. Because of the presence of many optical components the system is less suitable than piezoresistive or interferometric detection for low temperature usage. The alignment of the laser beam on the cantilever and the reflected beam on the photodiode is to be maintained. This proves to be very difficult. If the low temperature adjustment of these components is intended it has to be fully remote controlled because the access to optical components is not available[62] (This is one of the reasons why we did not choose this method for our low temperature MFM head). Theoretically it has been shown that under optimal conditions beam-bounce deflection is just as sensitive as the interferometric detection.[67] It was further shown that from a physical point of view, both methods are equivalent. For this the authors argued that the laser beam of the optical beam-bounce detection reflecting from the cantilever is equivalent to the interference of the two laser beams, one at the base of the cantilever while the other at the tip. In a way similar in the interferometric detection, the displacement of the tip results in shifting the interference pattern, thereby giving the means to measure the signal. Therefore the expression for the signal-to-noise ratio for the two systems is also similar.

b. Optical detection with all fiber construction or fiber-optic interferometer

   The optical detection with all fiber construction works on the principle of a Fabry-Perot interferometer. It can be described with the help of Fig. 11.
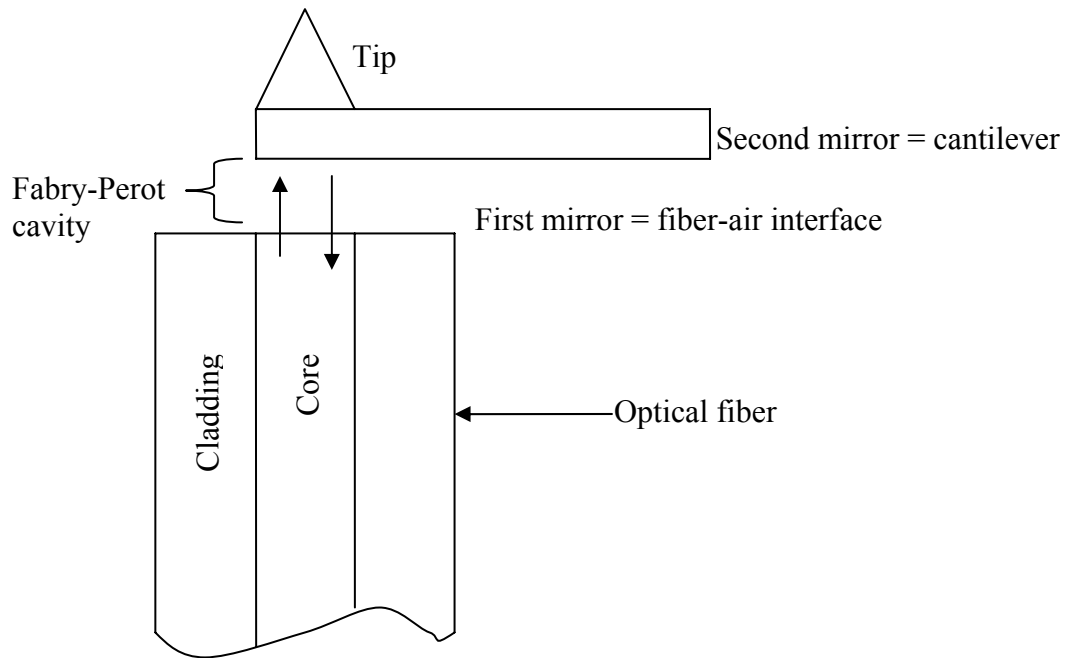
FIG. 11. Principle of the fiber-optic detection method

   The optical fiber lying very close (typically within half a μm) to the back of the cantilever forms a part of the Fabry-Perot cavity. The first mirror is formed by the fiber-air interface where around 4 % of the light is reflected back into the fiber forming the first interferometer beam. The other mirror is the back of the cantilever which reflects light back toward the fiber. The interference between the first beam and this reflected light which goes back into the fiber gives the interferometer signal. This signal is a function of the distance between the cantilever and the fiber.

c. Homodyne detection

   The principle of operation of this method is explained nicely in reference 2. In the homodyne detection system, a polarized laser beam is passed through a beam splitter.

The undeflected beam is incident in the optical cavity formed by the back of the cantilever and an optical flat. The reflected beam also passes through the same beam splitter and then onto the photodiode. This generates a photocurrent used to image the force acting on the tip. In the improved differential detection, two beam splitters are used. The first one diverts a portion of the beam called the reference beam which goes directly to the reference photodiode. The second beam splitter carries the undeflected portion of the laser beam which goes to the cavity formed by the backside of the cantilever and an optical flat. The reflected beam goes back to the second photodiode called the signal photodiode. The difference in the photocurrents of these two photodiodes is the required signal. The differential operation helps to cancel the laser noise. A system using just one photodiode but otherwise similar to the one described above was also used.[68] Use of a phase sensitive detector is also an option. This method is also suitable for contact and non-contact modes. In AC mode the photodiode generates a current at the frequency at which the cantilever is vibrated.

The presence of many mechanical components makes this system susceptible to drift related problems. Use of a fiber coupled laser reduces the possibility of instability due to differences in optical path length.[69] The all-fiber construction eliminates the problem altogether though the principle of operation is same. In general the interferometric technique provides an absolute calibration of cantilever deflection, using the laser wavelength as a reference. Such a feature is important for quantitative measurements.[70]

d. Heterodyne detection

This method was first used in 1987.[63] There are two beam splitters in this system. The first beam splitter divides the light into two components. One of the beams passes through an acousto-optic modulator that shifts the beam frequency. The other part is reflected onto a mirror and is used as a reference beam. The beam with the shifted frequency is the signal beam. It is further passed through a polarizing beam splitter, a quarter-wave plate and lastly through a microscope objective that focuses it onto the back of the cantilever. The lever reflects the beam back through the microscope

objective and quarter-wave plate. Then it again goes back through beam splitter and an analyzer that adjusts the relative power of the beam incident on the photo detector. The reference beam is deflected by two mirrors, passes through the beam splitter and an analyzer to fall back on the photo detector. These two interfere to form interference pattern consisting of a spectrum of frequencies. The photo current is fed into a single side-band receiver driving a phase-sensitive detector that provides the signal for the force detection. The phase locked loop (PLL) has been used for this purpose.[16]

Heterodyne detection has a distinct advantage over homodyne detection in that it is immune to the time dependent drift in the optical path length.[63] The resolution and sensitivity is comparable to the homodyne detection scheme.

These are just a few of the detection methods employed over the years. There are other less commonly used systems such as capacitance detection (useful for electric force microscopy), polarization detection, laser diode feedback detection which are not discussed. These days majority of the researchers prefer either the optical beam-bounce or fiber interferometric detection system as their methods of choice. The obvious reason is that the optical beam-bounce is very simple and easy to use while fiber-optic interferometer is very suitable for special cases such as low temperature environments.

B. DESIGN OF THE FIBER-OPTIC INTERFEROMETER

In our MFM head design a fiber-optic interferometer sensor is used for measuring cantilever deflection. The fiber-optic interferometer detection is advantageous for cryogenic use because only a single fiber runs down the length of the cryostat. The advantage of running only the fiber along the length of the microscope is that it reduces the sensitivity of the sensor to the electrical pick-up and the temperature extremes encountered in the microscope. All the electronics stays outside. Moreover the adjustment of the fiber is not as critical as in the case of tunneling.[62] The interferometer schematically shown in the Fig. 11, is suitable for both dc and ac modes of force microscopy. As a result of using a laser diode as a light source and all-fiber construction, the sensor is compact, mechanically robust and exhibits good low-frequency noise behavior. There is no air path between optical components (except for the micron-sized

path between the cleaved end of the fiber and the cantilever); the instrument is much less susceptible to instabilities caused by air currents and acoustic noise. The peak to peak noise in a DC to 1 kHz is less than 0.01 nm as reported routinely by various groups.

One of the first instances of use of this design was in 1993.[71] The basic construction and working of the interferometer can be explained as follows. A multimode laser [Appendix 1] with single mode fiber [Appendix 1] is used as a light source. The laser diode we have used operates at 1310 nm wavelength, has a power rating of 3 mW, and is powered by a precision current source [Appendix 1] from Thorlabs Inc. A stable current source for the laser diode helps to avoid damage due to current spikes. The light is coupled into a 2×2 single mode directional coupler [Appendix 1] through a Faraday isolator [Appendix 1]. The signal from one arm of the coupler is used as a reference and goes into the reference photodiode [Appendix 1]. The other arm carries the light to the fiber end and cantilever. Approximately 4% of the light is reflected from the glass-air interface at the cleaved end of the fiber (earlier called the fiber-air interface). The rest of the light is carried into the cavity between the fiber end and the back of the cantilever. This beam impinges on the back of the cantilever and a part of it is scattered back into the fiber. The beam reflected from the fiber-air interface and the beam scattered from the back of the cantilever form an interference pattern. This is the output signal which goes into the signal photodiode.

The photodiodes we have used have an active area of diameter 80 μm and responsivity of 1 A/W at the laser frequency. The power reaching the reference photodiode is on the order of 250 mW (equivalent to a current of 250 mA), and the power reaching the signal photodiode is on the order of 50 mW (equivalent to a current of 50 mA). The current signals from both the photodiodes are converted into amplified voltages (hereafter referred to as signal and reference voltage respectively) using low noise OP-AMPS [Appendix 1] in trans-impedance configuration as I-V converters. The signal voltage from the signal photodiode can be directly used in the feedback circuit. The laser diode noise is prominent at low frequencies. This can be cancelled by subtracting the reference voltage from the signal voltage. The resulting signal is further

amplified using a low noise instrumentation amplifier [Appendix 1] in differential mode to match it with the input level of the Dulcinea electronics which is the commercial electronics box we use to control the scanner. This signal is used to drive the feedback circuit as well as form the images.

The schematic of the fiber-optic interferometer, the signal processing circuit board and its interfacing scheme are shown in the Figs. 12 and 13 respectively.
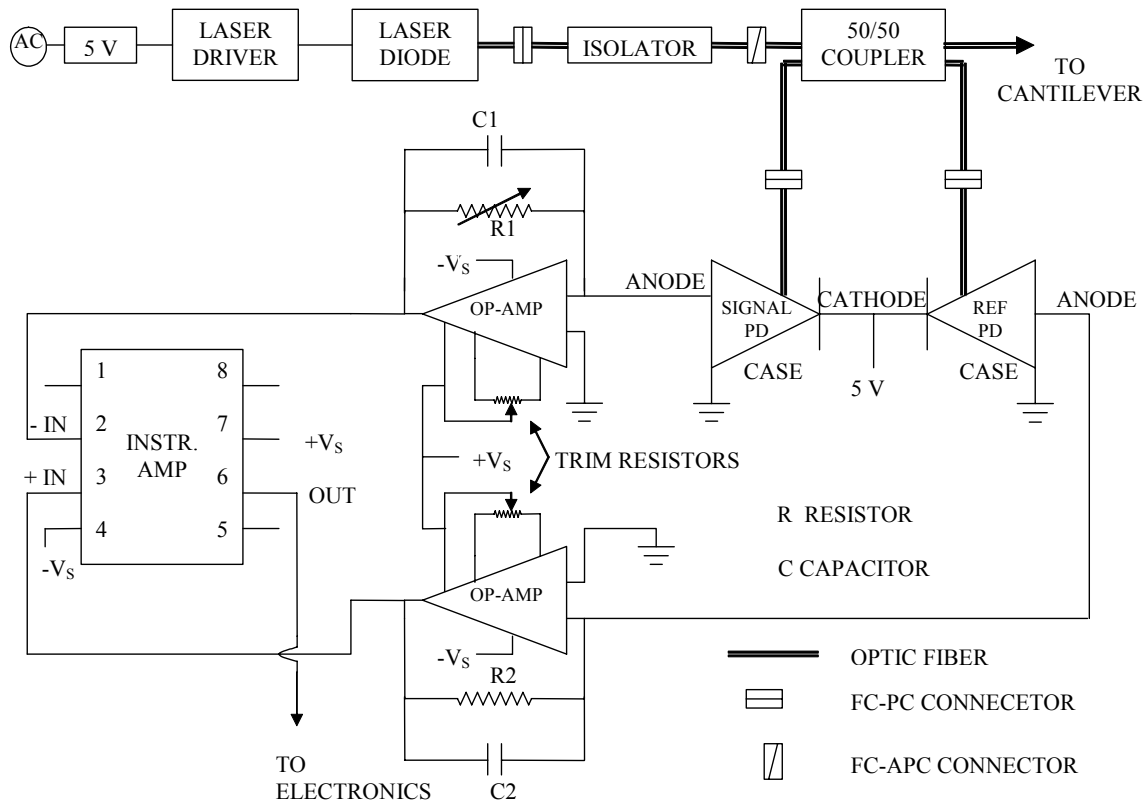
FIG. 12. Schematic of the fiber-optic interferometer and the circuit board
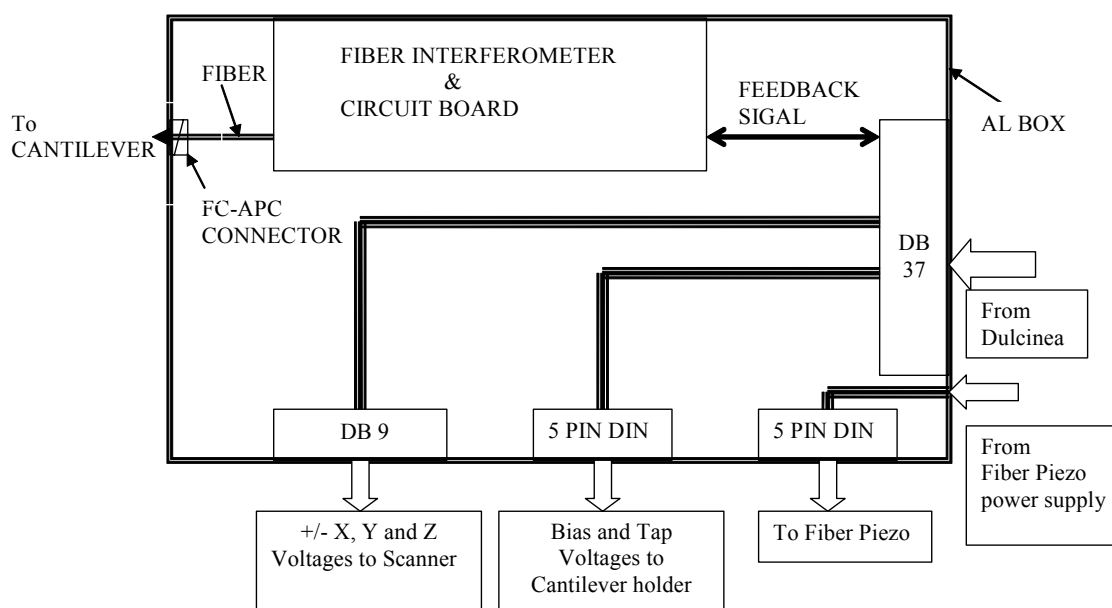
FIG. 13. Interface box

The current design includes many improvements over the first one. For e.g. in the earlier designs conventional lasers were used. In such instruments the low frequency noise is because of the phase noise and the noise due to stray reflections. Using a diode laser helps because its coherence length can be small compared to conventional lasers.[72] The laser diode we have chosen also has very small coherence length of 1.7 mm. Associated with a laser there is inherent noise due to unwanted back reflections. The Faraday isolator prevents reflections from filtering back into the laser diode. The isolator was used for the first time in 1993.[71] The Faraday isolator is insensitive to mechanical vibrations and does not complicate the operation of the SFM. Also, with the Faraday isolator any cantilever can be used in any position since the back reflections no longer matter. Use of the directional coupler helps by reducing the birefringence introduced by fiber bends. Thus it does not disturb the operation of the sensor. The fiber length in the each arm of the directional coupler is kept intentionally different to decrease the relative coherence of the residual stray reflections from the fiber ends.[73] APC connectors which

have fiber-air junctions intentionally cut at an angle) are used instead of PC at places wherever possible. This helps to reduce the noise due to stray reflections of light at the fiber-air interface inside the different connectors. Since light emerging at an angle from FC-APC connectors can miss the sensitive area of the photodiode detectors, signal loss was reduced by using a non-angled connection (FC-PC) to connect the fiber to the photodiode.

The response of the interferometer has been described by various mathematical models. In the simplest case interferometer response can be modeled as a simple two component interference since multiple reflections in the interferometer cavity can be ignored due to relatively low reflectivity. The current from the signal photodiode is given by

$$i \approx i_o \left(1 - V \cos \frac{4\pi d}{\lambda} \right), \tag{19}$$

where λ is the laser wavelength and d is the fiber to cantilever spacing. V is the fringe visibility given
by

$$V = \frac{\left(i_{max} - i_{min} \right)}{\left(i_{max} + i_{min} \right)}, \tag{20}$$

where i_o is the midpoint current given by [72]

$$i_o = \frac{\left(i_{max} - i_{min} \right)}{2}. \tag{21}$$

The most sensitive operating point is where the phases of the two reflected components are in quadrature or *d=λ/8, 3λ/8, 5λ/8...* At quadrature, the response for small changes in distance, Δd, and wavelength, $\Delta \lambda$, is given by

$$\frac{\Delta i}{i_o} = 4\pi V \frac{\Delta d}{\lambda} - 4\pi d V \frac{\Delta \lambda}{\lambda^2}. \tag{22}$$

The power variation at this point is given by the linear relation

$$P_{out} = P_0(1 - 4\pi\overline{V}\Delta d / \lambda)$$ (23)

where $\overline{V} = \dfrac{V_{max} - V_{min}}{V_{max} + V_{min}}$.[74]

In general if the interferometer distance is set to its most sensitive point, the force resolution of the microscope only depends on the force constant of the cantilever used and on the resolutions of the interferometer optical system.

There are some miscellaneous issues regarding the operation of fiber-optic interferometer which are worth mentioning. The active core diameter of the fiber is about 5-10 μm (8.3 μm in our case) and SFM cantilevers are generally only a few hundred microns long and a few tens of microns wide. Thus precise positioning of the optical fiber over the cantilever and easy cantilever replacement are thus major concerns in any interferometer design.[75] In our system this is done at room temperature with the help of an optical microscope. While looking through the microscope the stainless steel plate on which the cantilever sits is positioned with the help of tweezers so that the cantilever is above the fiber in X-Y plane. The spacing between the cantilever and the fiber along the Z-axis is maintained as small as possible. This is later readjusted for the final positioning.

The more critical requirement for the low temperature design is maintaining adequate alignment while cooling to low temperature.[76] Since no provision is made for lateral re-alignment of the fiber and cantilever after cooling in our instrument, fiber alignment done at room temperature must be maintained throughout the cooling process. To achieve this, misalignment of the cantilever and fiber due to thermal contractions is minimized by the symmetric design of the cantilever and fiber-positioning mechanisms. These components are laterally symmetric about an axis along the length of the cantilever. With this geometry, thermal contractions result in relative motion of the fiber and cantilever which has virtually no component in the X-Y plane perpendicular to the axis of the cantilever.[73] However, in the Z-direction, relative motion of several microns

may occur upon cooling despite the thermal compensation described below. Thus it is necessary to perform final approach of the cantilever and sample at low temperature.[70] In our instrument this is done using one screw for the coarse approach and the fiber piezo for fine approach. In practice while doing the final adjustment, the fiber is typically brought up to the cantilever until it just touches (oscillations stop) the fiber. Then the fiber is backed by a micrometer or so as necessary to be at the most sensitive part of the signal curve (i.e. where the distance is a multiple of $\lambda/8$). However, the stability of the microscope is always limited by the Z-drift of the cantilever to fiber spacing.

The fiber is very susceptible to breaking during adjustment, so the fiber needs to be strain relieved close to its end. Our first approach was to use a ceramic ferrule separated from the standard FC-PC fiber connector as the fiber supporting capillary. However, to make this approach successful the fiber needs to be stripped free of its plastic coating (which increases its susceptibility to breaking manifolds). This bare fiber is glued 'inside' the ferrule which makes the ferrule useless if the fiber breaks. To avoid this we have now used hypodermic stainless steel tubing as a fiber supporting capillary through which the fiber can be passed with its plastic coating intact. With this method, it is necessary to glue the fiber only at the base of the tubing and the steel tubing itself can be easily replaced. Virtually any length of the fiber can be used between the active components and the interferometer cavity, which is simply formed by reflections between the cleaved fiber end and reflective back surface of the cantilever. Every time the fiber breaks the end of the fiber is cleaved accurately perpendicular, using a commercial cleaving tool.

The subtraction approach for the noise reduction mentioned earlier is advantageous only in the contact mode. In the frequency range important for the contact mode, laser shot noise may be significant and this is reduced by the subtraction approach. On the other hand, in the frequency range important for the AC mode, the noise level of the interferometer is limited by the thermal noise of the cantilever which exhibits a peak near resonance as is always the case in AC mode.

This noise is relatively large in the range of 10^{-3}-10^{-1}Å$/\sqrt{\text{Hz}}$ [72] at room temperature compared to the shot noise of the laser diode given by[69]

$$(2eSP_{avg}\Delta f)^{1/2} , \tag{24}$$

where S is detector responsivity in (Å/W) and is independent of the frequency of the cantilever.

The next section describes the issues in the design of any MFM system in general and actual design of our MFM head based on these design parameters.

IV. MFM HEAD DESIGN

A. FUNDAMENTALS

Ever since the introduction of scanning force techniques a decade ago, a substantial amount of effort has been made to use them not only at room temperature and atmospheric pressure, but also in high vacuum and at low temperatures. Though MFM has produced very interesting images at room temperature and atmospheric pressure, working under the above special conditions has advantages.

Advantages of using a vacuum environment:

In high vacuum conditions relatively clean surfaces can be prepared and imaged. Moreover the quality factor of the cantilever increases substantially which helps in increasing the strength of the signal. Piezoelectric positioners have a tendency to arc usually between the pressures of 1 torr and the millitorr region because of the high voltage applied, so having a high vacuum environment ensures safe working conditions for the piezo material.

Advantages of working at low temperature:

Operating at low temperatures has the advantages of improved signal-to-noise ratio, elimination of thermal drift, increased stability, and the possibility of investigating low temperature phenomena. The signal to noise ratio increases because the amplitude of the cantilever's thermal noise decreases as $\sqrt{T}$. To put that into perspective, at LN_2 temperatures the thermal noise reduces by a factor of 2 and data collection is 4 times faster than at room temperature. Not only does the thermally activated drift of the mechanical construction decrease as temperature decreases, but the creep of the piezo and hence image distortions also decrease. Furthermore, interesting low temperature phenomena which are exclusively accessible only to low temperature MFM include superconductivity, many magnetic phase transitions and surface diffusion of molecules.[77]

Various designs for the MFM working in these conditions have been proposed. Each has its own particular characteristics because of different: a) methods of scanning the sample and tip with respect to each other,[64, 78] b) systems used to measure the

cantilever deflection, c) range of operating temperatures and pressures,[79] d) scanning ranges, e) size, shape, material and construction of the instrument, f) cost and optimization of the use. Thus it is difficult to compare one design with another. There are still new designs emerging with their own advantages and limitations.

The design of a magnetic force microscope has requirements which differ in certain respects from those of the design of a generic atomic force microscope. The magnetostatic interaction produces forces and force gradients considerably smaller than produced by van der Waals forces so MFM requires a deflection sensor of good stability and low noise characteristics. Also though atomic resolution is not essential in AFM, a large scan range is required to study micromagnetic features and relate them to topographical features.[80] Scanning force microscopes invariably have modular design due to its obvious advantages. Our MFM head has several modules. The starting point for the design process was several previously reported designs.[40, 72, 81] In this work, I have combined and improved upon, various features of these designs. Specifically, I used AutoCAD as the drafting software for this design work, and 2-D views were used to establish the proper geometry and alignment of the various parts inside each module and the modules themselves. Most of the parts for each module were manufactured in the physics workshop. Individual modules and the MFM head were assembled in Dr. Ross' lab. In the end, except for some minor adjustments individual modules and the head as a whole has thus far worked as we had planned.

In the following section, the various issues, parameters and constraints involved in the MFM head design are discussed with respect to each module. Then each of our modules is described on the basis of relevant design parameters.

B. DESIGN ISSUES IN GENERAL

The capability for low-temperature operation places additional requirements on the design of the instrumentation, in addition to any room temperature requirements. Low temperature systems can be built with a vacuum environment without exchange gas. In a vacuum environment such as this, temperature control issue is more critical because there is no fluid to exchange the heat. The method of heat transfer is either conduction or radiation.

The prominent issues are mechanical stability, spurious mechanical resonance frequency and external vibration sensitivity. The suggestions of M. D. Kirk et al.[9] as follows: 1) elimination of differential thermal contractions which could cause misalignment of the cantilever and the detection mechanism (in our case the optical fiber) 2) small size and rigid construction to enable the instrument to fit into a helium dewar with minimal vibration isolation 3) an ultra fine mechanical approach system to accommodate the reduced response of the piezoelectric transducers at low temperatures. The combined problem of vibration isolation and cooling is harder to solve than either problem alone. The vibration isolation/damping can be introduced either inside the cryostat just for the microscope or outside the entire cryostat. For immersion microscope with a vacuum environment (as is the case with this MFM) outside vibration isolation is a practical solution. However, effective vibration decoupling of gas and vacuum lines is required to achieve noise free cryostat operation.

Proper control of the actual tip and sample temperature can be very hard to achieve. Thus the aim of any design is to make the head compact. The small size not only makes the instrument rigid but also reduces thermal mass. Our MFM head has an outside diameter of 5 cm. This compact design ensures the necessary rigidity.

Any scanning force microscope working at low temperatures should be symmetric about the cantilever. This helps in minimizing the problem of unequal contraction of the parts while cooling to low temperature. At temperatures well below the LN2 temperature, expansion coefficients tend to decrease to practically zero,[82] so the only differential contraction problem for very low temperature operation is the shift

during cooling. Thus a thermally compensated design simplifies the approach. This feature is also present in our MFM head.

The coarse sample approach and the coarse fiber approach in our case are manual. This eliminates the use of a motor and makes the design simple, with little compromise in functionality. A key design challenge was to make the head thermally stable with low drift by thermally compensating the important parts. The design incorporated a fiber-optic interferometer sensor, which is most convenient in high vacuum and low temperature environments. Thus this choice of deflection sensing method relieved us of other constraints on the design of this MFM.

The cantilever holder is capable of using different commercial cantilevers. This feature should prove useful to investigate samples with widely varying properties. We have used a super-insulated dewar [Appendix 1] as a bath cryostat for low temperature operation. Vibrations produced by a bath cryostat are much lower than a flow cryostat. Other advantages of a bath cryostat are low LHe consumption and no sample contamination from residual gases due to the cold environment. The sample handling or microscope handling itself becomes difficult as the sample sits at the bottom of a long tube. In our case, since the microscope was not designed for the in-situ exchange of the sample, this issue is not important.

One of the advantages of a super-insulated dewar is elimination of noise created by boiling nitrogen which is required for cooling. Noise from boiling helium can be eliminated by pumping the helium bath temperature below λ point[77] or temporarily by over-pressuring the bath. This MFM works in the dynamic detection mode which has higher sensitivity than the DC mode. It is possible to use stiff cantilevers which are easier to stabilize at low scan heights.

C. DESIGN AND FEATURES OF INDIVIDUAL MODULES

1. Sample coarse approach

This is a manual approach. For this design, ultra fine screws [Appendix 1] are used to achieve as small a step as possible. These screws rest on a plate called the 'Lower Plate' which houses the scanner on which the sample rests. The material of the main body, which includes three plates as well as the coarse approach screws of the microscope, is non-magnetic 304-stainless steel. Using non-magnetic construction materials is imperative for MFM and choosing an appropriate material of construction was one of the design challenges. A survey of available construction materials revealed that materials like Invar have much lower thermal contraction coefficients (needed for low temperature operation), but they are useless for our purpose because they are magnetic while the inverse is true for materials like plastics. Comparison of the relative merits and demerits of different materials is shown with the help of table I, which gives the values of relative thermal contraction for different materials and compares the properties of these materials with those of stainless steel.

TABLE I. Liner thermal contraction of materials at 60 K relative to 293 K (adapted from G.K. White, Experimental Techniques in Low Temperature Physics, Oxford Science Publications, 1987) in units of $10^4 \times (L_{293} - L_T)/L_{293}$ and comparison of different materials with stainless steel based on suitability as a material of construction for MFM

Material	Relative thermal Contraction	Comparison with S. Steel
Stainless Steel	29.1	------------
Aluminum	40.6	Higher thermal contraction
Copper	31.2	Lower strength and rigidity, comparable thermal contraction
Titanium	14.8	Lower thermal contraction, higher cost and difficult to machine
Invar	4.9	Lower thermal contraction, magnetic
Plastics	>100	Higher thermal contraction
Macor	approx. 5	Very low tensile strength, very difficult to machine
EBL-3	approx. 5	Piezoceramic material, not a material for bulk construction

This is why we have used 304-stainless steel (which is non-magnetic for all practical applications and has relatively lower coefficient of thermal contraction) as the material of construction for the main body.

The sample approach screws are accessible from outside the vacuum with the help of the long screwdriver. The screwdriver shafts are made to have good thermal contact with the cold vacuum can which serves as the heat sink for the heat conducted along their length.

2. Fiber coarse approach

This also features a manual approach mechanism similar to the sample coarse approach mechanism and has the same material of construction. These ultra fine screws pass through a plate called the 'Upper Plate' and rest on a plate called the 'Middle Plate'.

The 'Upper Plate' houses the fiber inside the fiber piezo. The 'Middle Plate' houses the cantilever on an angled slot milled at its center. One of the fiber approach screws is accessible from outside the vacuum. This screw also sinks its heat to the cold vacuum can. Thus we have tried to minimize the thermal path from cantilever to the optical fiber to optimize resolution and stability. Drift is also minimized because of the use of materials having similar expansion coefficients (e.g. piezo ceramic and macor).[79, 83] It was expected that lateral thermal drift of the fiber with respect to the cantilever would be minimal due to the symmetric design of the instrument.[70] Hence there is no provision for the lateral alignment of the fiber and cantilever as is already discussed in detail section 3.

3. Scanner piezo

The single tube piezo scanner is a common feature in any SFM system. It has the distinct advantage of being small and rigid as compared to other piezo based motors. Our piezo tube is made of EBL-3 [Appendix 1], which has the highest gain (d_{31}) of 26.2 Å/V.[84] The length of the tubes (L) chosen is 7.5 cm, one of the longest ever reported. The thickness (d) is chosen to be small (0.5 mm). The scanning range for the piezos can be given by[85]

$$\Delta x \, or \, \Delta y = (2\sqrt{2} * d_{31} * V * L^2)/(\pi * ID * d) \, . \tag{25}$$

From equation (25) it can be easily seen that the scanning range is directly proportional to gain and length and is inversely proportional to thickness. That is why we have chosen the piezo material with highest gain and the length of the tubes is kept long. The scanning range also depends on the value of the electric field (V/d) applied. With our electronics we can apply voltages up to +/- 300 V. Value of the typical breakdown voltage (or more correctly field) for the piezo materials is 1000 V/mm. So the smallest value for the thickness (d) of the piezo tubes we could have chosen would be around 0.3 mm. However, the piezo tubes are very fragile, so the thickness of the tubes was chosen to be 0.5 mm due to strength considerations. This strength consideration proved to be very useful during the assembly as we found that even with 0.5 mm thickness the piezo tubes should be handled very carefully to avoid breaking.

This four quadrant scanner is used for the final approach of the sample and scanning as well. A single four-quadrant scanner tube is usually used to raster the sample with respect to cantilever or vice versa. Our scanner has concentric piezo tubes to effectively improve the scanning range (the scanning range at room temperature is $175 \times 175 \ \mu m$). At low temperatures the scanning range of the piezo tubes decreases by a large amount (reduction factors of 3-8 have been reported[76, 86]). This has been compensated by concentrically mounting two piezo tubes and connecting them in parallel. The arrangement of concentric piezo tubes is also useful for thermal compensation of the scanner in two ways: 1) the relative contraction of piezoceramic material from room temperature to 60 K is approximately 1/6 that of stainless steel [Table 1] which is the material of the main body of the MFM head. This large difference can introduce unwanted thermal stresses in the scanner. It can also increase the chances of accidental contact of the cantilever and the sample while cooling the head (explained in detail in subsection 5 which discusses design of the sample holder) 2) the relative contractions of piezoceramic material and macor (from which the supporting flanges for the scanner are made) are only approximately the same. However, for a large scanner length of 7.62 cm the resulting difference in contraction is still significant. The concentric tubes along with the similar macor flanges contract relative to each other by equal amount thereby minimizing the above mentioned problems. We are not aware of any other reported design of the scanner with thermal compensation achieved in this way.

On top of the scanner piezo sits the sample holder, with the help of the sample holder macor flange. A SS plate is glued to this macor flange on which the sample holder attaches. Thus sample holder is removable if needed.

4. Fiber piezo for the fine adjustment

The fiber fine adjustment is done by two concentric single quadrant piezo tubes [Appendix 1]. These tubes hold the optical fiber [Appendix 1], at their common center with the help of a macor flange and a hypodermic steel tube fitting. The fiber is glued to the hypodermic steel tube to provide the fiber with a strain relief which prevents frequent breaking. Although a long piezo is essential for sufficient extension, in this case

the length of the z-piezo could not be too large because of our geometrical constraint. The fiber piezo should be perpendicular to the tilted cantilever, so it was placed at an angle of 15^U with respect to the Z-axis of the microscope. To confine it inside the diameter of the microscope, the length of the fiber piezos chosen is 2cm (the Z-extension of the fiber piezos is 20 μm at room temperature). These piezos sit in a macor base flange clamped to the 'Upper Plate'. The thermal expansion coefficient of both these materials (i.e. macor and EBL-3) is the same which avoids problems during the cooling process.[86]

5. Sample holder

The sample holder sits on the scanner between the 'Middle Plate' and the 'Lower Plate'. These two plates are separated by coarse approach screws which are made of stainless steel and are 7.62 cm long. Because of the geometry of the Scanner module of our MFM head, the sample holder sticks out above the 'Lower Plate'. During cooling of the head the 'Lower' and the 'Upper' plates move toward each other by a large amount (proportional to the relative thermal contraction of stainless steel) while sample holder does not contract as much (here, the contraction is proportional to the relative thermal contraction of piezo material EBL-3 and is very small) and still sticks out almost as much as it does at room temperature. This can be compensated if the sample holder itself contracts by a large amount. This is the reason the sample holder is made of aluminum and its height is chosen to be 2.54 cm. The relative thermal contraction (compared to room temperature legth) of aluminum at 60 K is 150% of the relative thermal contraction of stainless steel and 800% of that of piezoceramic material [Table 1]. Hence based on the values of relative thermal contraction between room temperature and 60 K, it compensates for 3.5 cm (=2.54×41.2/29.1) length of the stainless steel approach screws. [Here, we had to compensate only for the coarse approach screws and not also the scanner because the scanner has already been thermally compensated as explained in subsection 3. Otherwise the relative contraction (at 60 K) of the scanner itself would be considerable]. This thermal compensation is very essential to avoid any accidental contact between the cantilever and the sample during cooling.

The sample holder has a fixture to hold the sample up to approximately 2.5cm by 2.5cm .The sample is held in its place by Cu-Be spring fingers. The sample holder was designed to allow attachment of a small heater to it if needed.

6. Cantilever holder

The cantilever holder consists of two very thin ceramic plates (approx. of size 1cm by 1 cm and 0.001 cm thick) which clamp the thin piezo plate. This piezo plate [Appendix 1] vibrates the cantilever near its resonant frequency for non-contact imaging. The lower thin ceramic plate is glued to an angled step machined in the 'Middle Plate'. The angle maintained is 15°. This tilts the cantilever towards the sample to allow only a corner of the lever to interact with the sample and to provide sufficient clearance for the approach. The cantilever is glued onto a thin stainless steel plate which is then held onto the upper ceramic plate with the help of Cu-Be spring fingers.

The next section describes the assembly of the MFM head and working of the magnetic force microscope.

D. ASSEMBLY AND WORKING

The assembly of the MFM head begins with gluing corresponding macor parts on to the respective piezo tubes. The macor parts are glued using Torr Seal [Appendix 1] and are fixed permanently. The two lower macor parts are used to couple the inner and outer tubes for fiber piezo assembly and also for scanner assembly. Macor base flanges are used to attach the scanner assembly to the 'Lower Plate' (Fig. 14) and the fiber piezo assembly to the 'Upper Plate' (Fig. 15).

52

FIG. 14. Scanner module assembly

Clearance Slot for
1/4-80 Screws

Tapped Holes for
3/16-100 Screws

#8-32 Tapped
Holes

Holes for the
Spring Support

Center Hole for
Piezo Tubes

Fiber Piezo
Supporting Plate
(S. Steel)

Inner lower
flange (macor)

Outer lower
flange (macor)

Top Plate
(S. Steel)

Outer Piezo
Tube (PZT)

Spring Support

Inner Piezo
Tube (PZT)

Fiber holder
macor flange

Fiber base
flange (macor)

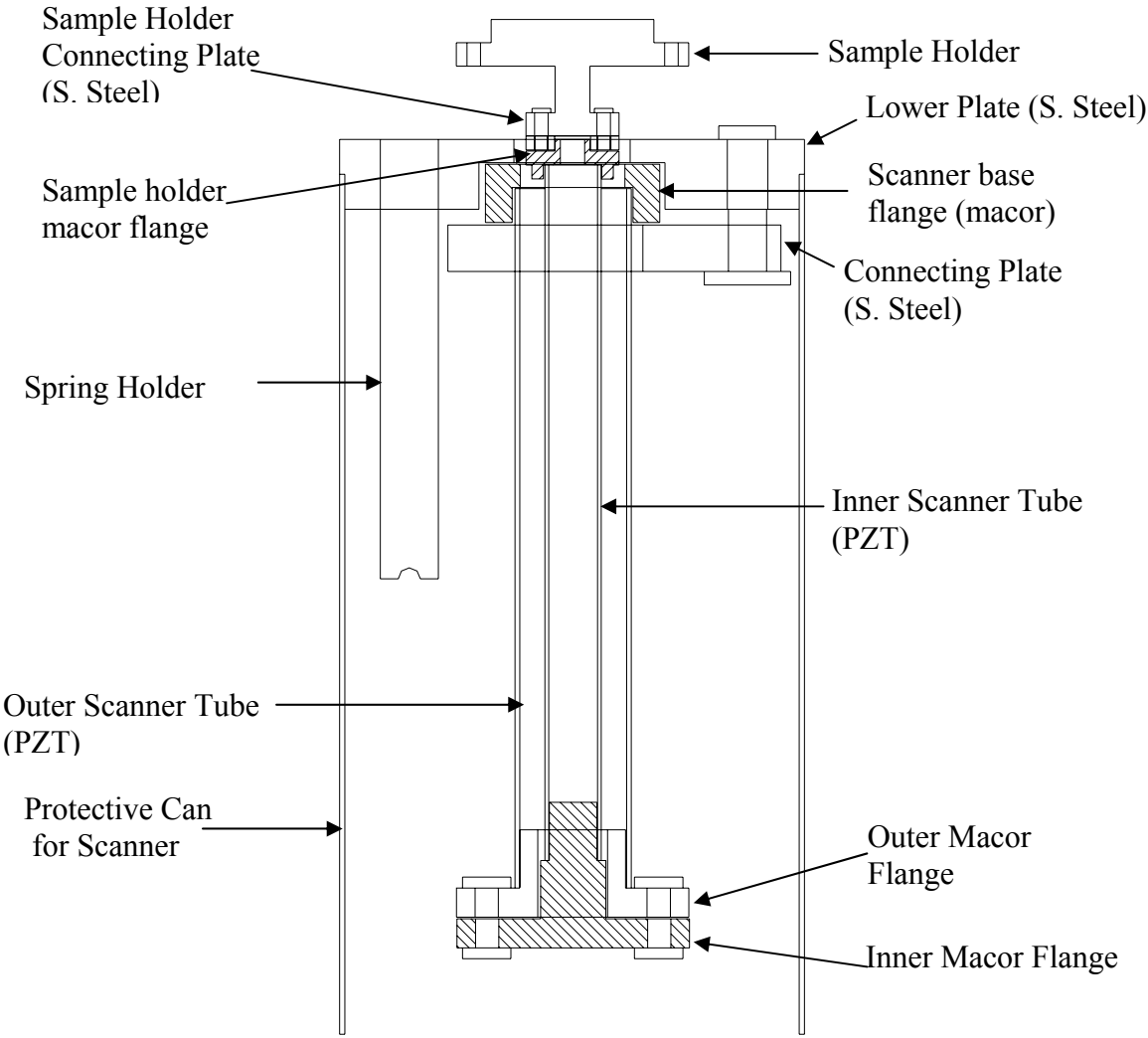Optic-Fiber
at 15^0
to the Z axis

Steel Plates and
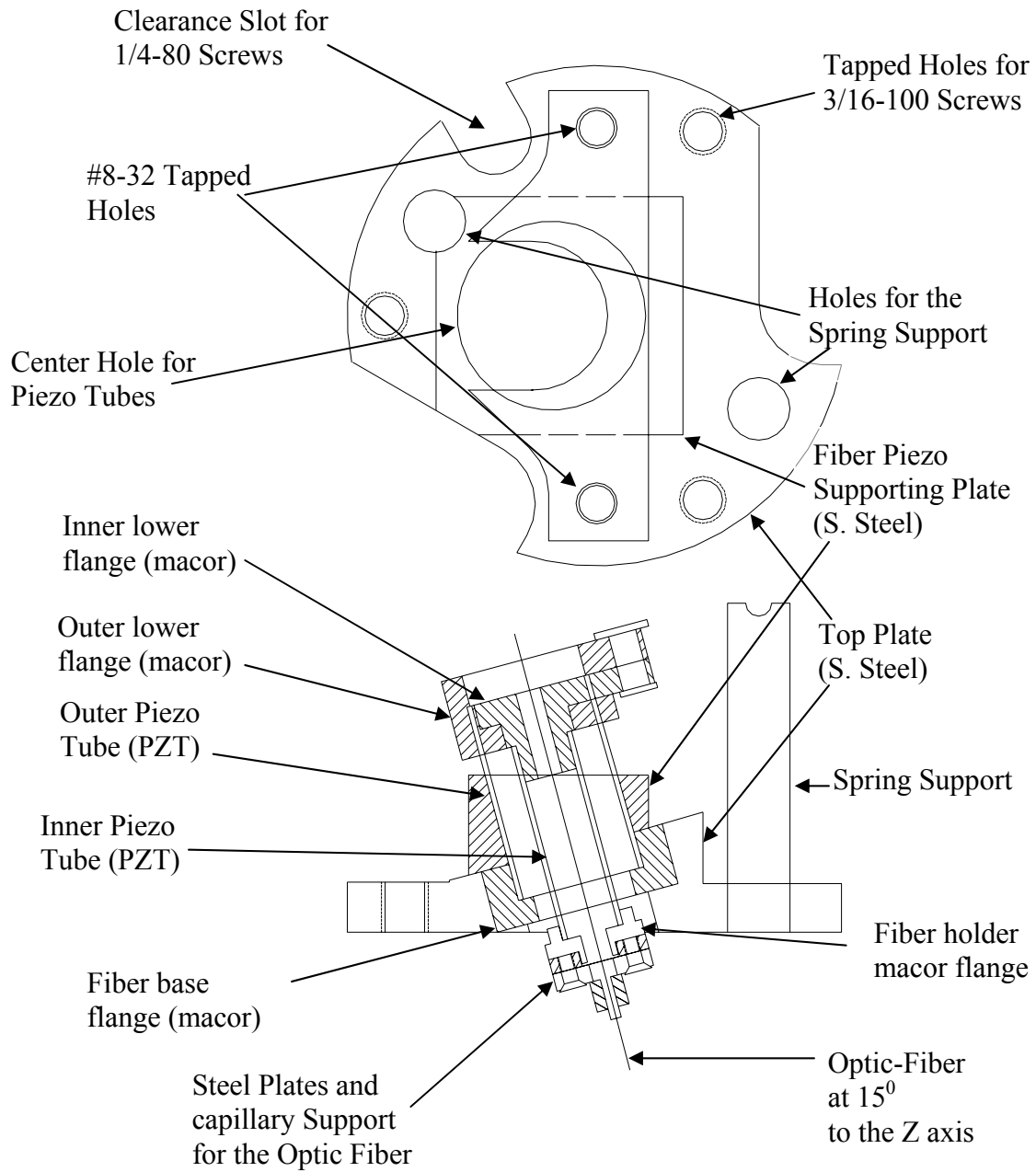capillary Support
for the Optic Fiber

FIG. 15. Fiber piezo module assembly

Additional macor flanges combined with small stainless steel plates with threading are attached to the inner scanner and fiber piezo tubes to carry the sample holder and capillary support for the fiber. The sample holder is screwed onto the scanner tube and the spring supports are placed in appropriate grooves in the 'Lower Plate'. The optical fiber is cleaved and then glued into the capillary support which then sits on top of the fiber piezo assembly.

To assemble the cantilever holder module, the small piezo plate is sandwiched between ceramic insulators and glued to the 'Middle Plate'. The cantilever is glued to a small stainless steel carrier and this is held to the ceramic insulator using Cu-Be spring fingers (Fig. 16). Then the Cantilever Holder module with the cantilever and the Fiber Piezo module with the coarse approach adjustment screws and fiber are tied together using springs. Room temperature alignment of the fiber is done using an optical microscope as described in section 3B. Then the Cantilever Holder module is attached to the Scanner module using springs. The 'Middle Plate' is screwed onto the Exterior Plate via Support Columns (Fig. 17) and thus remains fixed while the 'Upper' and 'Lower' plates are adjusted.

During the routine operation of the MFM, the coarse approaches move the Fiber Piezo module and the Scanner module relative to the 'Middle Plate'. Movement of the Scanner module moves the sample towards the cantilever housed in the 'Middle Plate'. Similarly movement of the Fiber Piezo module moves the fiber towards the cantilever from its other side. This will bring the sample and the fiber piezo within the range of the fine approaches. The fine approach is then used to move within the range of the feedback signal which forms the image.

The three screws for the scanner approach and one screw for the fiber approach are accessible from outside. For this, four long screwdriver rods passing through 0.63 cm thin walled Cu-Ni tubes are used (Fig. 18). The Cu-Ni tubes are soldered at one end onto the Exterior Plate while at the other end are held onto the Ladish Flange 1 using Quick Connectors. Thus the Exterior Plate along with the whole assembly of the MFM head can be moved up and down using these tubes. The Ladish Flange 1 mates with the Ladish Flange 2 as shown in Fig. 19. The Ladish Flange 2 is soldered onto a S. Steel tube which in turn is soldered onto a flange on one side. On the other side a vacuum can (6.35 cm in diameter and approximately 100 cm long) is soldered below the stainless steel tube. This assembly is placed in the superinsulated dewar to immerse the MFM head enclosed in the vacuum can in the cold liquid. A KF-20 flange soldered onto the S. Steel tube provides access for the vacuum pumping system as shown in Fig. 20. Ladish Flange 1 has Quick Connectors for various vacuum feedthroughs. Similarly the flange sitting on top of the dewar also has additional vacuum feedthroughs for purposes such as LN_2 or LHe transfer.

The optical fiber is glued into a plug and is held onto the Ladish Flange 1 using a Quick Connect. The optical fiber is connected to the Interface Box as shown earlier and carries the feedback signal to and from the Dulcinea electronics.

The electrical connections for the scanner and the fiber piezos are shown schematically if Fig. 21.

Clearance Slots for wires etc.

Slots for holding Springs

V-shaped Slots to support Screws

Tapped holes for 1/4-80 Screws

3/16-100 S. Steel Screws to move the Fiber Piezo

Thin piezo plate sandwiched between the ceramic plates

Middle Plate (S. Steel)

Z

Y X

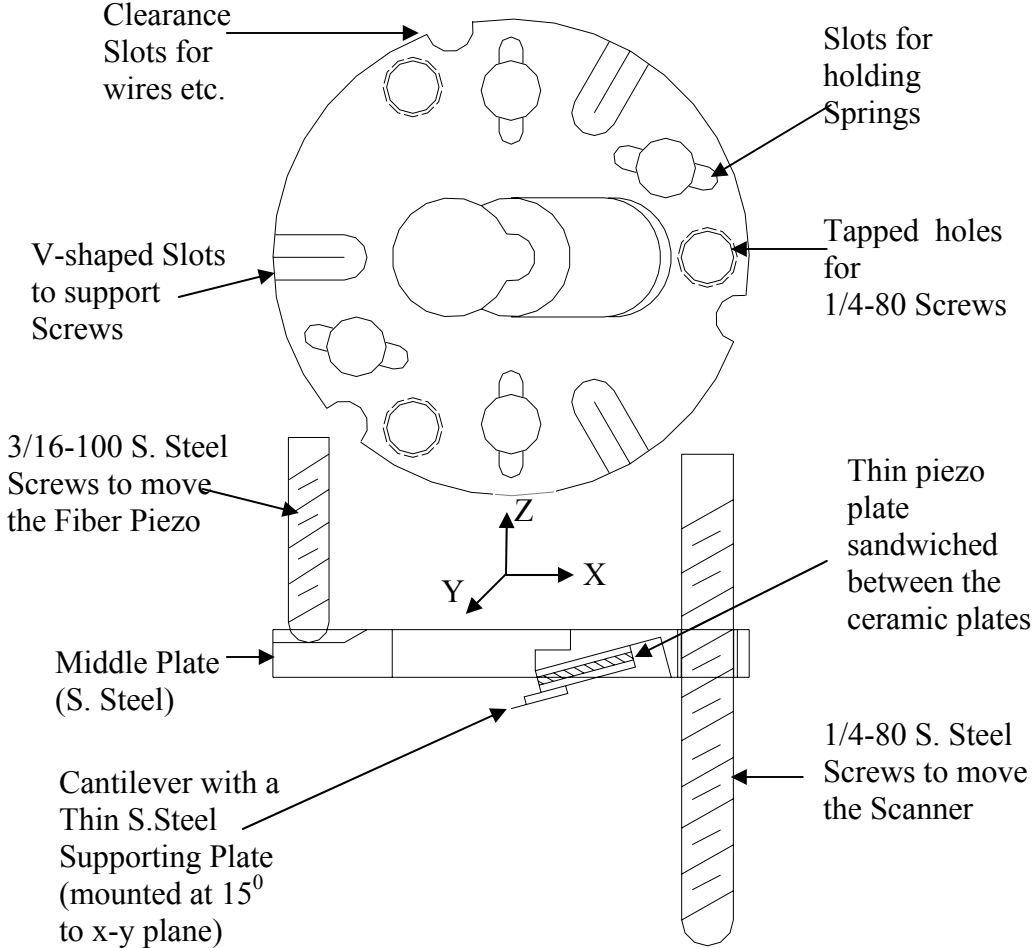Cantilever with a Thin S.Steel Supporting Plate (mounted at 15^0 to x-y plane)

1/4-80 S. Steel Screws to move the Scanner

FIG. 16. Cantilever holder module assembly
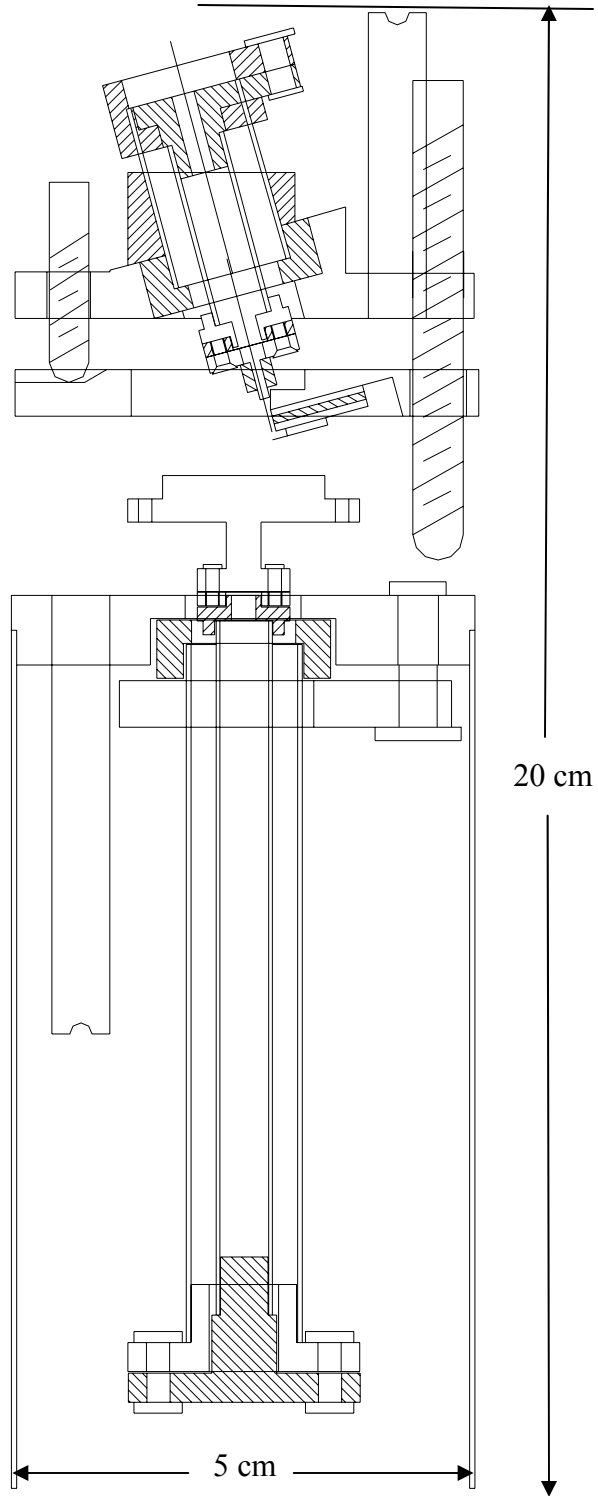
FIG. 17. Head assembly, showing 3 modules combined to form the MFM head

Screwdriver passing through 0.63 cm thin walled Cu-Ni Tube

Exterior Plate

Support Column

Fiber Piezo assembly

Upper Plate….Moves down towards the Middle Plate

Middle Plate…Fixed to the Exterior Plate

Lower Plate…Moves up towards the Middle Plate

0.63 cm Tubes are Soldered at 4 places on the Exterior Plate

1/4-80 Screw

Sample Holder

Scanner module
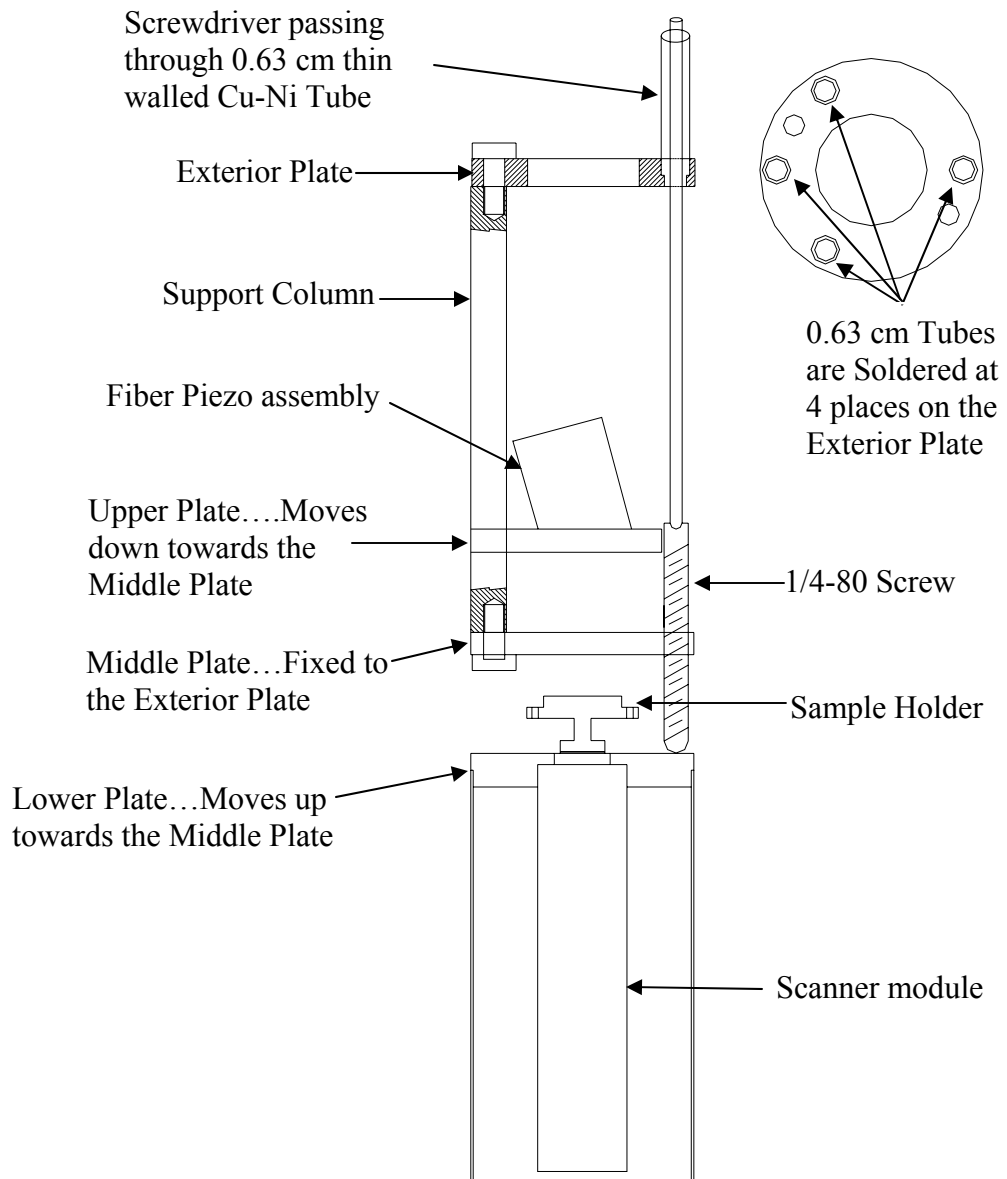
FIG. 18. Probe assembly 1, showing the MFM head assembled to the Exterior Plate

Screwdriver

Optic Fiber glued to a Plug sits
in Quick Connector

Quick
Connectors (4)

Quick
Connectors (4)

Quick
Connectors (2)

Ladish Flange 1

0.63 cm
Thin
Walled
S. Steel
Tubes (4)

Exterior Plate

Support Column

Optical
Fiber
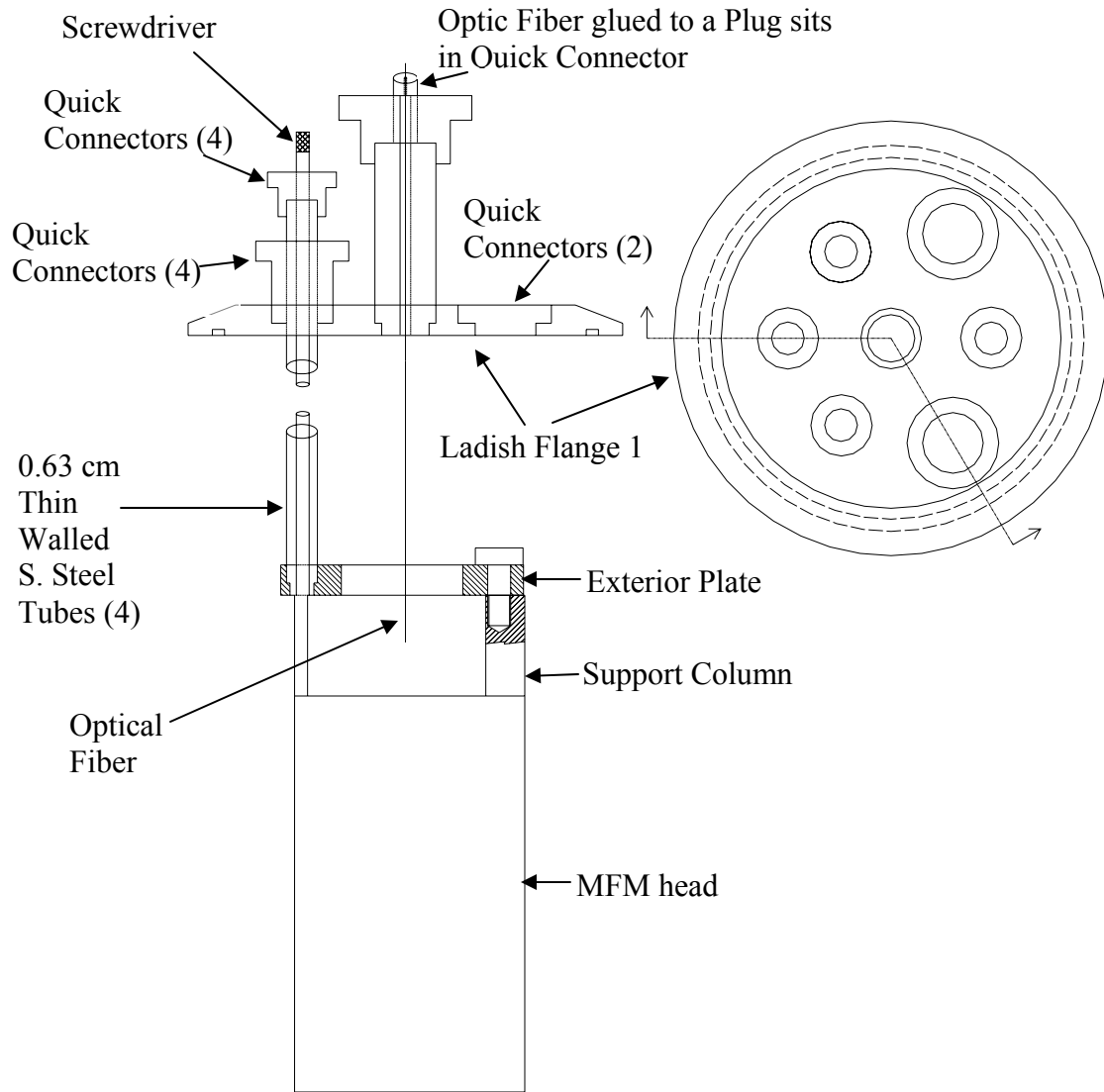
MFM head

FIG. 19. Probe assembly 2, showing the MFM head alignment with Ladish Flange at top

60

Ladish Flange 1
carrying the MFM head
mates here1

Ladish Flange 2

Quick Connectors for
Feedthroughs

0.63 cm Pipe
Threaded Connector

KF-20 Flange for
Vacuum Pump

Flange

O-ring Groove
on the dewar

Superinsulated
Dewar

6.35 cm Dia. Thin
walled S. Steel Tube
Vacuum Can
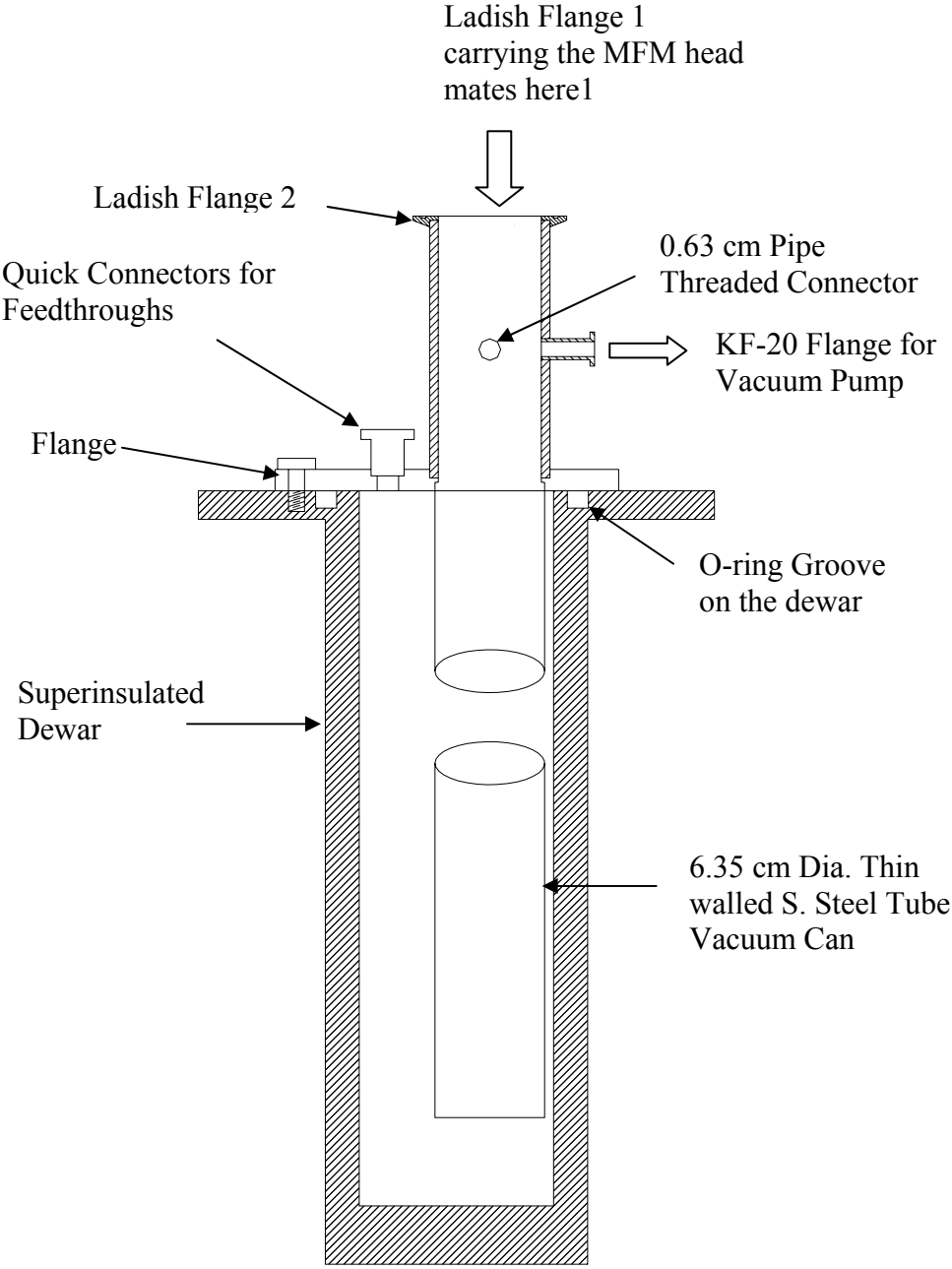
Fig. 20. Vacuum-can assembly with superinsulated dewar

Fiber Piezos

Inner piezo tube

-Z

+Z

Outer piezo tube

Scanner Piezos

Inner piezo tube with
four quadrants

+ X

-Z

+ Y

-Y

Outer piezo tube with
four quadrants

- X
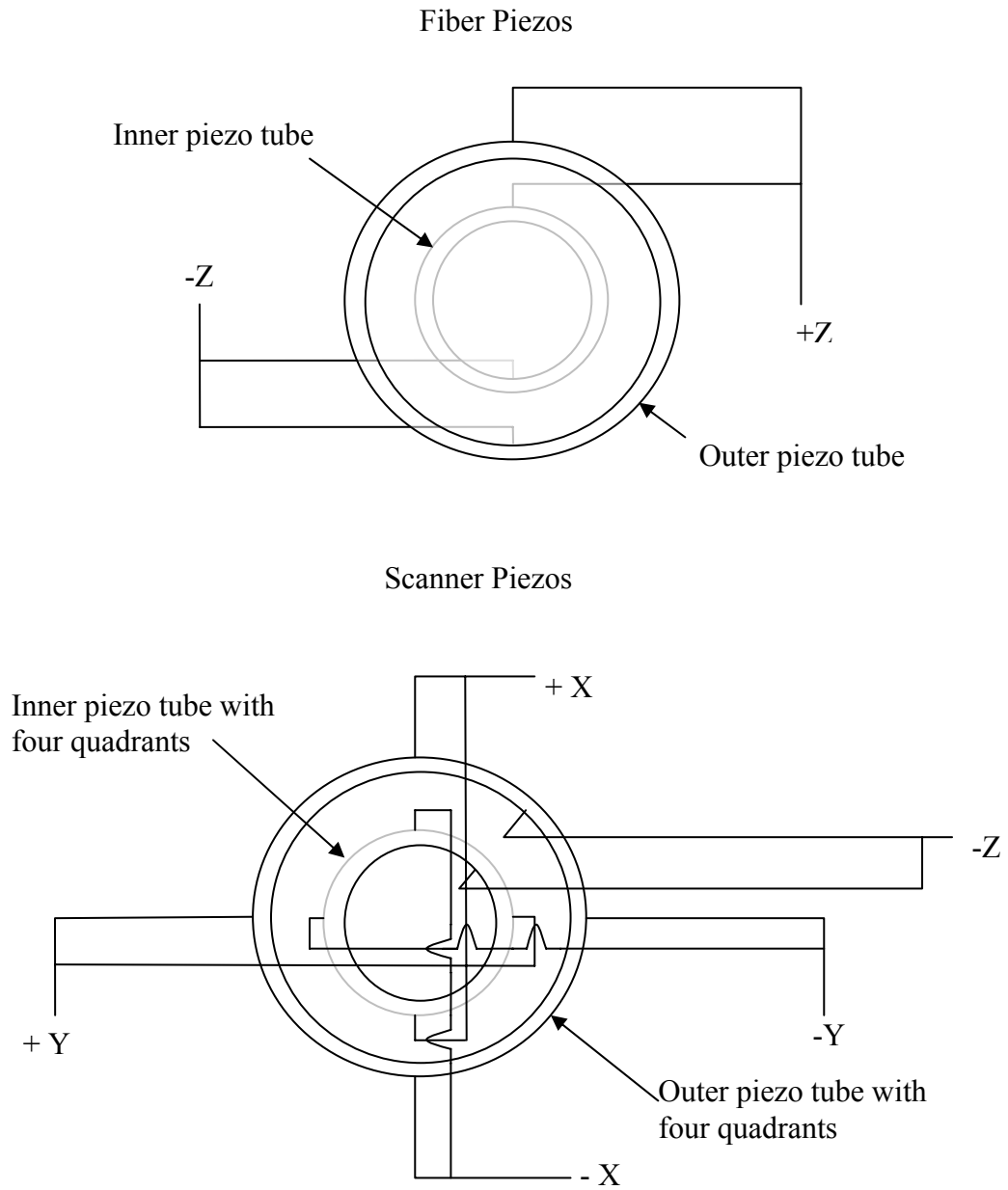
FIG. 21. Electrical connections for the scanner and the fiber piezos

E. FURTHER WORK AND APPLICATIONS

The design of the MFM head and interface is complete. The various modules have been manufactured. Now, they are in the assembly stage. Immediate further work involves calibration of this system at room temperature and at low temperature.

After the MFM head has been tested with the standard samples during calibration, it would be ready to be used for various investigative purposes at room temperature as well as at low temperature. The potential samples are the Mn_{12} molecular nanomagnets, Ni-Co-Al smart materials, BSCCO superconductors and Alumina based magnetic nanorods-superconductor hybrid structures. Mn_{12} molecular nanomagnets have a superparamagnetic transition temperature far below room temperature and MFM imaging of these samples around this temperature would be interesting. Ni-Co-Al smart materials show changing magnetic response with changing temperature so these are to be imaged while cycling through a certain temperature range. BSCCO superconductors are to be used to study the flux pinning with the help of the vortices and they have the transition temperature of around 77K. Alumina based hybrid structures have a layer of superconductor overlaid on Ni based magnetic nanorods embedded in Alumina. The ferromagnetic properties of the nanorods and their interaction with the superconductor below the transition temperature are to be studied

V. SUMMARY

In this project, a MFM head was designed and constructed. This MFM head works at low temperature (up to 4 K) and in high vacuum. It sits at the bottom of a 100 cm long vacuum can which is inserted into a superinsulated dewar for the cooling purposes. This cools the whole MFM head instead of just the sample as is the case with the cold finger arrangement. This helps to keep the sample clean as the sample no longer behaves as a cold trap. The MFM head was designed to be compact (outside dia. 5 cm) and hence fits into a 5.3 cm bore of the 9T superconducting magnet in Dr. Ross' lab. This feature is necessary for MFM imaging in high external applied fields (in the range of a few Teslas). The small size ensures small thermal mass for the ease of cooling.

The MFM head has various other features. It consists of various modules for ease of assembly. It is symmetrical in shape which minimizes uneven thermal contraction during cooling. This ensures reliable and stable operation over a range of temperatures. Most of its important modules are thermally compensated thereby making it suitable for low temperature operation. Its metal parts are made of non-magnetic stainless steel. It has a large scan range which is a very useful feature for a MFM system. Our MFM head uses commercially available magnetic cantilevers and is interfaced to a commercial electronics package, the Dulcinea unit made by Nanotec Electronica, Spain.

The interfacing was done by designing a fiber-optic interferometer as the deflection sensor and an interface box which goes with it. The fiber-optic interferometer is the most suitable sensor for a low temperature such as this because only the fiber runs into the low temperature part. The fiber-optic interferometer is compact, stable, less susceptible to mechanical vibrations and easy to use.

AutoCAD was used as the drafting software for designing various modules. 2-D drawings were used to ensure proper geometry and spatial compatibility as alignment and lack of space were the major design constraints. These various modules were manufactured in the Physics machine shop. The MFM head was assembled in Dr. Ross' lab by combining these modules and they work as intended. The assembly of the fiber-optic interferometer and the interface box is also complete. Now this home made MFM

head is ready to be interfaced to the commercial electronics package, the Dulcinea. This new head has many potential MFM imaging applications which were previously impossible to image in our lab. Some of the expected system specifications are once again listed as follows: 1) Outside diameter of the MFM head: 5 cm, 2) room temperature scanning range: 175 μm, 3) low temperature scanning range: 35-50 μm, 4) smallest detectable magnetic force in the range of pN, 5) smallest detectable magnetic force gradient in the range of 10^{-3} to 10^{-5} N/m, 6) lateral resolution on the order of a few nm depending on the imaging conditions and 7) vertical resolution on the order of a few Å depending on the imaging conditions.

REFERENCES

[1] G. Binnig, H. Rohrer, Ch. Gerber and E. Weibel, "Surface studies by scanning tunneling microscopy", Phys. Rev. Lett. **49**, 57 (1982)

[2] G. Binnig, C. F. Quate and Ch. Gerber, "Atomic force microscope", Phys. Rev. Lett. **56**, 930 (1986)

[3] U. Hartmann, "Fundamentals and special applications of non-contact scanning force microscopy", Adv. In Electronics and Electron Physics **87**, 49 (1994)

[4] U. Hartmann, "An elementary introduction to atomic force microscopy and related methods", http://www.uni-saarland.de/fak7/hartmann/download/afm/afm.pdf, (1997)

[5] Y. Martin, C. C. Williams and H. K. Wickramsinghe, "Atomic force microscope- force mapping and profiling on a sub-100 Å scale", J. Appl. Phys. **61**, 4723 (1987)

[6] T. R. Albrecht, P. Grutter, D. Horne and D. Rugar, "Frequency modulation detection using high-Q cantilevers for enhanced force microscope sensitivity", J. Appl. Phys. **69**, 668 (1991)

[7] C. B. Prater, P. G. Maivald, K. J. Kjoller and M. G. Heaton, "Tapping mode imaging applications and technology", http://www.veeco.com/appnotes/AN04_TM_GEN.pdf, (1998)

[8] Y. Martin and H. K. Wickramsinghe, "Magnetic imaging by 'force microscopy' with 1000 Å resolution", Appl. Phys. Lett. **50**, 1455 (1987)

[9] C. Schoenberger, S. F. Alvarado, S. E. Lambert and I. L. Sanders, "Separation of magnetic and topographic effects in force microscopy", J. Appl. Phys. **67**, 7278 (1990)

[10] J. J. Saenz, N. Garcia, P. Grutter, E. Meyer, H. Heinzelmann, R. Wiesendanger, L. Rosenthaler, H. R. Hidber and H. J. Guntherodt, "Observation of magnetic forces by the atomic force microscope", J. Appl. Phys. **62**, 4293 (1987)

[11] A. Moser, H. J. Hug, B. Stiefel and H. J. Guntherodt, "Low temperature magnetic force microscopy on $YBa_2Cu_3O_{7-\delta}$", J. Magn. Magn. Mater. **190**, 114 (1998)

[12] H. J. Mamin, D. Rugar, J. E. Stern, B. D. Terris and S. E. Lambert, "Force microscopy of magnetization patterns in longitudinal recording media", Appl. Phys. Lett. **53**, 1563 (1988)

[13] R. Proksch, G. D. Skidmore, E. D. Dahlberg, S. Foss, J. J. Schmidt, C. Merton, B. Walsh and M. Dugas, "Quantitative magnetic field measurements with the magnetic force microscope", Appl. Phys. Lett. **69**, 2599 (1996)

[14] M. R. Freeman and B. C. Choi, "Advances in magnetic force microscopy", Science **294**, 1484 (2001)

[15] L. Folks and R. C. Woodward, "The use of MFM for investigating domain structures in modern permanent magnet materials", J. Magn. Magn. Mater. **190**, 28 (1998)

[16] P. C. D. Hobbs, D. W. Abraham and H. K. Wickramsinghe, "Magnetic force microscopy with 25 nm resolution", Appl. Phys. Lett. **55**, 2357 (1989)

[17] H. J. Mamin, D. Rugar, J. E. Stern, R. E. Fontana, Jr. and P. Kasiraj, "Magnetic force microscopy of thin permalloy films", Appl. Phys. Lett. **55**, 318 (1989)

[18] P. Grutter, A. Wadas, E. Meyer, H. R. Hidber and H. J. Guntherodt, "Magnetic force microscopy of a CoCr film", J. Appl. Phys. **66**, 6001 (1989)

[19] D. Rugar, H. J. Mamin, P. Guthner, J. E. Lambert, J. E. Stern, I. McFayden and T. Yogi, "Magnetic force microscopy: general principles and application to longitudinal recording media", J. Appl. Phys. **68**, 1169 (1990)

[20] H. V. Kuo, C. A. Merton and E. D. Dahlberg, "Magnetic force microscopy studies of bit erasure in particulate magnetic recording media", J. Magn. Magn. Mater. **226-230**, 2046 (2001)

[21] Y. Honda, N. Inaba, F. Tomiyama, T. Yamamoto and M. Futamoto, "Spectrum analysis of recorded magnetization using magnetic force microscopy", Jpn. J. Appl. Phys. **34**, L987 (1995)

[22] X. Yang, M. Maeda, M. Yasui, Y. Okumura and Y. Okawa, "MFM study of the effects of thickness and composition in high recording density CoCrTa/Cr media", J. Magn. Magn. Mater. **148**, 466 (1995)

[23] G. Bochi, H. J. Hug, D. J. Paul, B. Stiefel, A. Moser, I. Parashikov, H. J. Guntherodt and R. C. O'Handley, "Magnetic domain structure in ultrathin films", Phys. Rev. Lett. **75**, 1839 (1995)

[24] R. Giles, J. P. Cleveland, J. Manne, P. K. Hansma, B. Drake, P. Maivald, C. Boles, J. Gurley and V. Elings, "Non-contact force microscopy in liquids", Appl. Phys. Lett. **63**, 617 (1993)

[25] R. Proksch, E. Runge, P. K. Hansma, S. Foss and B. Walsh, "High field magnetic force microscopy", J. Appl. Phys. **78**, 3303 (1995)

[26] T. Chang and J. G. Zhu, "Angular dependence measurement of individual barium ferrite recording particles near the single domain size", J. Appl. Phys. **75**, 5553 (1994)

[27] A. Wadas and H. J. Hug., "Models for the stray field from magnetic tips used in magnetic force microscopy", J. Appl. Phys. **72**, 203 (1992)

[28] R. Weber, W. Mertin and E. Kubalek, "Voltage influence of biased inter connection line on integrated circuit-based current contrast measurements via magnetic force microscopy", Microelect. Reliab. **40**, 1389 (2001)

[29] Digital Instruments: Veeco metrology group, "Magnetic imaging: new techniques and applications", http://www.veeco.com/appnotes/AN29_Magimag.pdf, (1998)

[30] T. G. Sorop, C. Untiedt, F. Luis, M. Kroll, M. Rasa and L. J. Jongh, "Magnetization reversal of ferromagnetic nanowires studied by magnetic force microscopy", Phys. Rev. B **67**, 014402 (2003)

[31] D. Ruiz-Molina, M. Mas-Torrent, J. Gomez, A. L. Balana, N. Domingo, J. Tejada, M. T. Martinez, C. Rovira and J. Veciana, "Isolated single-molecule magnets on the surface of a polymeric thin film", Adv. Mater. **15**, 42 (2003)

[32] P. T. Lilliehei, C. Park, J. H. Rouse and E. J. Siochi, "Imaging carbon nanotubes in high performance polymer composites via magnetic force microscopy", NASA/CR-2002-212137, ICSE Report No. 2002-48, (2002)

[33] S. H. Chung, S. R. Shinde, S. B. Ogle, T. Venkatesan, R. L. Greene, M. Dreyer and R. D. Gomez, "Low temperature behavior of magnetic domains observed using a magnetic force microscope", J. Appl. Phys. **89**, 6784 (2001)

[34] H. J. Hug, A. Moser, Th. Jung, O. Fritz, A. Wadas, I. Parashikov and H. J. Guntherodt, "Low temperature magnetic force microscopy", Rev. Sci. Instrum. **64**, 2920 (1993)

[35] A. P. Volodin and V. Marchevsky, "Magnetic force investigation of superconductors: first results", Ultramicroscopy **42-44**, 757 (1992)

[36] H. J. Hug, A. Moser, O. Fritz, I. Parashikov, H. J. Guntherodt and Th. Wolf, "Low temperature magnetic force microscopy on high Tc-superconductors", Physica B **194-196**, 377 (1994)

[37] H. J. Hug, A. Moser, O. Fritz, I. Parashikov, H. J. Guntherodt and Th. Wolf, "Magnetic force microscopy on high Tc-superconductors", J. Vac. Sci. Technol. B **12**, 1586 (1994)

[38] F. Hellman, E. M. Gyrogy, D. W. Johnson, Jr., H. M. O'Bryan and R. C. Sherwood, "Levitation of a magnet over a flat type II superconductor", J. Appl. Phys. **63**, 447 (1988)

[39] P. Rice and J. Moreland, "Tunneling stabilized magnetic force microscopy of $YBa_2Cu_3O_{7-\delta}$ films on MgO at 76 K", IEEE Trans. Magn. **27**, 6 (1996)

[40] A. Moser, H. J. Hug, I. Parashikov, B. Stiefel, O. Fritz, H. Thomas, A. Baratoff, H. J. Guntherodt and P. Chaudhari, "Observation of single vortices condensed into a vortex glass phase by magnetic force microscopy", Phys. Rev. Lett. **74**, 1847 (1995)

[41] H. J. Hug, Th. Jung, H. J, Guntherodt and H. Thomas, "Theoretical estimates of forces acting on a magnetic force microscope tip over a high temperature superconductor", Physica C **175**, 357 (1991)

[42] C. W. Yuan, Z. Zheng, A. de Lozanne, M. Tortonese, D. A. Rudman and J. N. Eckstein, "Vortex imaging in thin films of $YBa_2Cu_3O_{7-x}$ and $Bi_2Sr_2Ca_1Cu_2O_{8+x}$ obtained by low-temperature magnetic force microscopy", J. Vac. Sci. Technol. B **14**, 1210 (1996)

[43] A. Volodin, K. Temst, C. V. Haesendock and Y. Bruynseraede, "Observation of the Abrikosov vortex lattice in $NbSe_2$ with magnetic force microscopy", Appl. Phys. Lett. **73**, 1134 (1998)

[44] A. Volodin, K. Temst, C. V. Haesendock and Y. Bruynseraede, "Imaging of vortices in conventional superconductors by magnetic force microscopy", Physica C **332**, 156 (2000)

[45] V. V. Moshchalov, "Vortex matter in superconductors at extreme scales and conditions: a scientific program of the European Science Foundation", Physica C **332**, ix (2000)

[46] M. Roseman, P. Grutter, A. Badia and V. Metlushko, "Flux lattice imaging of a patterned niobium film", J. Appl. Phys. **89**, 6787 (2001)

[47] M. Roseman and P. Grutter, "Estimating the magnetic penetration depth using constant-height magnetic force microscopy imaging of vortices", N. J. Phys. **3**, 24.1 (2001)

[48] M. J. Van Bael, M. Lange, L. V. Look, V. V. Moshchlkov and Y. Bruynseraede, "Vortex pinning in ferromagnet/superconductor hybrid structures", Physica C **364-365**, 491 (2001)

[49] M. J. Van Bael, L. V. Look, M. Lange, J. Bekaert, S. J. Bending, A. N. Grigorenko, K. Temst, V. V. Moshchlkov and Y. Bruynseraede, "Ferromagnetic pinning arrays", Physica C **369**, 97 (2002)

[50] M. J. Van Bael, S. Raedts, K. Temst, J. Swerts, V. V. Moshchlkov and Y. Bruynseraede, "Magnetic domains and flux pinning properties of a nanostructures ferromagnet/superconductor bilayer", J. Appl. Phys. **92**, 4531 (2002)

[51] M. Roseman and P. Grutter, "Determination of Tc, vortex creation and vortex imaging of a superconducting Nb film using low-temperature magnetic force microscopy", J. Appl. Phys. **91**, 8840 (2002)

[52] A. Volodin and P. Grutter, "Magnetic force microscopy of vortex pinning at grain boundaries in superconducting thin films", Physica C **369**, 165 (2002)

[53] A. de Lozanne, "Scanning probe microscopy of high temperature superconductors", Supercond. Sci. Technol. **12**, R43 (1999)

[54] D. Sarid, *Scanning Force Microscopy,* (Oxford University Press, New York, 1991)

[55] D. Pelekhov, J. B. Becker and G. Nunes, "Ultralow-temperature atomic force microscopy for the investigation of mesoscopic systems", Appl. Phys. Lett. **72**, 993 (1998)

[56] G. Binnig and H. Rohrer, "Scanning tunneling microscopy", IBM J. Res. Develop. **30**, 335 (1986a)

[57] P. Guthner, U. Ch. Fischer and K. Dransfeld, "Scanning near-field acoustic force microscopy", Appl. Phys. B **48**, 89 (1989)

[58] F. J. Giessibl and B. M. Trafas, "Piezoresistive cantilevers utilized for scanning tunneling and scanning force microscopy in ultrahigh vacuum", Rev. Sci. Instrum. **65**, 1923 (1994)

[59] C. W. Yuan, E. Batalla, M. Zacher, A. de Lozanne, M. D. Kirk and M. Tortonese, "Low temperature magnetic force microscope utilizing a piezoresistive cantilever", Appl. Phys. Lett. **65**, 1308 (1994)

[60] M. Tortonese, R. C. Barrett and C. F. Quate, "Atomic resolution with an atomic force microscope using piezoresistive detection", Appl. Phys. Lett. **62**, 834 (1993)

[61] J. Tansock and C. C. Williams, "Force measurement with a piezoresistive cantilever in a scanning force microscope", Ultramicroscopy **42-44**, 1464 (1992)

[62] H. J. Hug, B.Stiefel, P. J. A. van Schendel, A. Moses, J. Martin and H. J. Guntherodt, "A low temperature ultrahigh vacuum scanning force microscope", Rev. Sci. Instrum. **70**, 3625 (1999)

[63] Y. Martin, C. C. Williams and H. K. Wickramsinghe, "Atomic force microscope-force mapping and profiling on a sub 100-Å scale", J. Appl. Phys. **61**, 4723 (1987)

[64] G. Meyer and N. Amer, "Novel optical approach to atomic force microscopy", Appl. Phys. Lett. **53**, 1045 (1988)

[65] S. Alexander, L. Hellemans, O. Marti, J. Scheneir, V. Elings, P. K. Hansma, M. Longmire and J. Gurley, "An atomic-resolution atomic-force microscope implemented using an optical lever", J. Appl. Phys. **65**, 164 (1989)

[66] O. Marti, J. Colchero and J. Mlynek, "Combined scanning force microscope and friction microscopy of mica", Nanotechnology **1**, 141 (1990)

[67] C. A. J. Putman, B. G. de Groth, N. F. van Hulst and J. Greve, "A theoretical comparison between interferometric and optical beam deflection technique for the

measurement of cantilever displacement in AFM", Ultramicroscopy **42-44**, 1509 (1992)

[68] R. Erlandsson, G. M. Mcclelland, C. M. Mate and S. Chiang, "Atomic force microscope using optical interferometry", J. Vac. Sci. Technol. **A6**, 266 (1988)

[69] D. Rugar, H. J. Mamin, R. Erlandsson, J. E. Stern and B. D. Terris, "Force microscopy using a fiber-optic displacement sensor", Rev. Sci. Instrum. **59**, 2337 (1988)

[70] M. Roseman and P. Grutter, "Cryogenic magnetic force microscope", Rev. Sci. Instrum. **71**, 3782 (2000)

[71] A. Moser, H. J. Hug, Th. Jung, U. D. Schwarz and H. J. Guntherodt, "A miniature fiber optic microscope scan head", Meas. Sci. Technol. **4**, 769 (1993)

[72] D. Rugar, H. J. Mamin and P. Guthner, "Improved fiber-optic interferometer for atomic force microscopy", Appl. Phys. Lett. **55**, 2588 (1989)

[73] T. R. Albrecht, P. Grutter, D. Rugar and D. D. E. Smith, "Low temperature force microscope with all fiber interferometer", Ultramicroscopy **42-44**, 1638 (1992)

[74] K. J. Bruland, J. L. Garbini, W. M. Doughtery, J. H. Chao, S. E. Jensen and J. A. Sidles, "Thermal tuning of a fiber-optic interferometer for maximum sensitivity", Rev. Sci. Instrum. **70**, 3542 (1999)

[75] P. J. Mulhern, T. Hubbard, C. S. Arnold, B. L. Blackford and M. H. Jericho, "A scanning force microscope with a fiber-optic displacement sensor", Rev. Sci. Instrum. **62**, 1280 (1991)

[76] R. Euler, U. Memmert and U. Hartmann, "Fiber interferometer-based variable temperature scanning force microscope", Rev. Sci. Instrum. **68**, 1776 (1997)

[77] H. J. Hug, *Forces in Scanning Probe Methods* edited by H.-J. Guntherodt, D. Anselmetti and E. Meyer, NATO ASI Series E: Applied Sciences (Kluwer Academic Publisher, Netherlands, 1995)

[78] S. Howell, Ph.D. dissertation, "Electrostatic force microscopy studies of nanoscale systems", Purdue University, 2000

[79] H. J. Hug, Th. Jung and H. J. Guntherodt, "A high stability and low drift atomic force microscope", Rev.Sci. Instrum. **63**, 3900 (1992)

[80] M. S. Valera and A. N. Farley, "A high performance magnetic force microscope", Meas. Sci. Technol. **7**, 30 (1996)

[81] M. D. Kirk, T. R. Albrecht and C. F. Quate, "Low-temperature atomic force microscopy", Rev.Sci. Instrum. **59**, 833 (1988)

[82] P. Davidsson, H. Olin, M. Persson and S. Pehrson, "Design and operation of a low-temperature scanning tunneling microscope suitable for operation below at 1 K", Ultramicroscopy **42-44**, 1470 (1992)

[83] W. Allers, A. Schwarz, U. D. Schwarz and R. Wiesendanger, "A scanning force microscope with atomic resolution in ultrahigh vacuum and at low temperature", Rev. Sci. Instrum. **69**, 221 (1998)

[84] Staveley NDT technologies, "EBL lead zirconate titanate characteristics", http://www.staveleyndt.com/products/ebllzt.html, (2003)

[85] C. J. Chen, "Electromechanical deflections of piezoelectric tubes with quartered electrodes", Appl. Phys. Lett. **60**, 132 (1992)

[86] D. V. Pelekhov, J. B. Becker and G. Nunes, "Atomic force microscope for operation in high magnetic fields at millikelvin temperature", Rev. Sci. Instrum. **70**, 114 (1998)

APPENDIX 1

The MFM head was assembled from custom made parts manufactured in the Physics machine shop and commercial parts. This appendix lists most of the commercial parts used in the construction of the MFM head.

Part No.	Name	Product No.	Manufacturer
1	Multimode laser diode	ML725B8F	Thorlabs Inc.
2	Single mode fiber	SMF-28	Thorlabs Inc.
3	Precision Current Source (Laser Driver)	IP500	Thorlabs Inc.
4	50-50 Directional Coupler	10202A-50	Thorlabs Inc.
5	Faraday Isolator	4013SA	Thorlabs Inc.
6	FC-PC connector	30126D1	Thorlabs Inc.
7	FC-APC connector	30126F1	Thorlabs Inc.
8	Photodiode	FD80W	Fermionics Opt. Tech.
9	OP-AMP	LT1007CN8	Maxim Inc.
10	Instrumentation amplifier	AD621AN	Analog Devices Inc.
11	Superinsulated dewar	---	Precision Cryogenics Inc.
12	1/4-80 S. Steel screw	FAS300	Thorlabs Inc.
13	3/16-100 S. Steel screws	UFS100	Thorlabs Inc.
14	Lead-Zirconium-Titanate (Piezo tube material)	EBL-3	Staveley Sensors Inc.
15	Macor (machinable glass ceramic)	_____	Accuratus Ceramic Corporation
16	Torr Seal	9530001	Varian Vacuum Products Inc.

VITA

Name: Sameer S. Khandekar

Date of Birth: 10/03/1979

Education:

M.S   Mechanical Engineering, Texas A&M University   2004

B.E   Mechanical Engineering, Walchand College of Engineering   2001

Home Address:

Vadnaka, Bapat Ali, Chiplun 415605, India